NASA/TP–20240011436

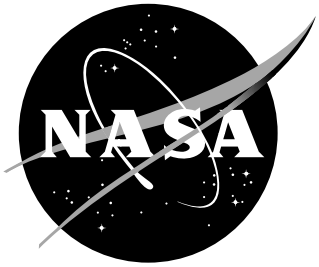

Final Report on Radiation Measurements Performed Inside of the BEAM Module

D. Fry, T. Campbell-Ricketts, R. Gaza, S. George, J. Keller, E. Semones and N. Stoffle
Space Radiation Analysis Group
NASA Johnson Space Center, Houston TX 77058

M. Kroupa
Los Alamos National Laboratory
Los Alamos, NM 87545

R. T. Bigelow and C. A. Kelleher
Bigelow Aerospace
Las Vegas, NV 89032

September

NASA STI Program ... in Profile

NASA/TP—-20240011436

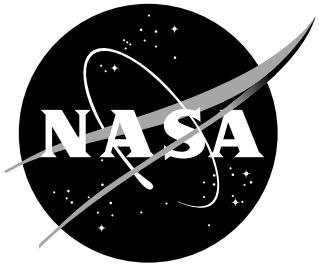

Final Report on Radiation Measurements Performed Inside of the BEAM Module

D. Fry, T. Campbell-Ricketts, R. Gaza, S. George, J. Keller, E. Semones and N. Stoffle
Space Radiation Analysis Group
NASA Johnson Space Center, Houston TX 77058

M. Kroupa
Los Alamos National Laboratory
Los Alamos, NM 87545

R. T. Bigelow and C. A. Kelleher
Bigelow Aerospace
Las Vegas, NV 89032

National Aeronautics and
Space Administration

Johnson Space Center

September

Acknowledgments

Work supported by NASA Johnson Space Center, the NASA International Space Station Program and the NASA Advanced Exploration Systems (AES) Program.

This report is available in electronic form at
http://

Abstract

Contents

List of Figures

List of Tables

1 Overview

Measurements of the radiation environment inside of the Bigelow Expandable Activity Module (BEAM) have been made on a pseudo-continuous basis since June 6, 2016 using both passive and active instrumentation. Passive detectors yield a single cumulative dose value (or average daily dose) over the measurement period from deploy to return to ground. Active Radiation Environment Monitor (REM) sensors yield dose rate, Linear Energy Transfer (LET) spectra, and particle-specific dose, all on a 1-minute cadence. From the initial install in 2016 until early 2018, BEAM was an empty module. In 2018, further testing was approved and stowage began to be moved into BEAM. As a result, it was decided to stop measurements with RAM detectors to avoid potential difficulties with access after stowage was added. The REM sensors remained however in the original deploy locations.

From the perspective of crew health and safety, it is important to separate out different parts of the particulate radiation field in both ion species and energy. The trapped belts, and in particular the South Atlantic Anomaly (SAA) are composed primarily of electrons and protons. The Galactic Cosmic Ray (GCR) component is comprised of protons and high-Z ions with energies exceeding several GeV per nucleon, n. The difference in energy spectrum and spatial distribution is modulated by Earth's geomagnetic field, and hence can be delineated to some degree by the latitudinal and longitudinal positioning of the International Space Station (ISS). Analysis of measurements taken inside of BEAM and other ISS modules has been partitioned this way based upon ISS latitude and longitude, magnetic rigidity cutoff, and energy deposition within the detector. This allows for separation of dose and dose rate in terms of South Atlantic Anomaly (SAA) and upper latitude components. The later contains particles constituting the Galactic Cosmic Ray (GCR) environment in Low Earth Orbit. The fundamental quantities measured with the REM sensors are deposited energy in silicon and track length on a per-charged particle basis. These are then used to derive LET, absorbed dose (D_{Si}) and dose rate ($\dot{D}_{Si}$).

The radiation environment inside of BEAM exhibits higher dose rates as compared to those measured in other habitable areas of the International Space Station (ISS) which contain more stowage (mass). Measurements from the REM units in BEAM suggest trapped protons in the SAA are the primary contributors to the elevated dose rates.

It is important from a crew risk perspective to understand the cause of the increase in dose rate inside of BEAM. If it is predominantly due to high-energy ions, Blood Forming Organs (BFOs) can be at higher risk of damage. However, if the increase is due to low-energy ions, energies where penetration into the human body is limited to relatively shallow depths, the risk is lower since the increase in dose is limited essentially to the skin. It is also important to note that the BEAM module is being demonstrated in an empty configuration and not expected to be used in this fashion in the future. Because of the low mass that shields the inner habitable volume, the increase in dose rate observed is expected to be an upper threshold to what would be seen with a module filled with necessary equipment.

Measured dose rates inside of BEAM at upper latitudes are more similar to

measurements in other ISS modules but slightly lower by about a 10% percent. We have however instituted a second way to segment the data. Using known cutoffs used to describe different regions of the geomagnetic field, we have separated out measurements occurring at upper latitudes from those at lower latitudes. Whereas the upper latitude daily dose continues to trend at roughly the sample magnitude as the sensor in the US LAB, the lower latitude daily dose is observed to be about 40% lower. The cause for this decreased continues to be investigated.

It must be stressed here that all measurement results for the time frame from initial deploy to early 2018 relate only to BEAM in an empty configuration. It is not expected to be operated in this fashion if used for human exploration and thus only provides a baseline of shielding effectiveness for the BEAM pressure shell. Furthermore, the analysis presented here is not in any way meant to judge the capability of BEAM to protect human crews in a pass/fail fashion. The goal of the measurements is only to assess the radiation shielding characteristics of the module and compare to what we know of shielding characteristics of ISS.

2 Hardware Deployment and Timeline

Two new REM sensors, S/N 2002 (chip ID H06) and S/N 2003 (chip ID H10) were launched on the Orbital ATK OA-6 vehicle arriving at ISS on March 26, 2016. H06 was deployed in ISS NOD1 and H10 in ISS NOD2 after arrival. Activation and checkout of the sensors was conducted for approximately 6 weeks. Both sensors displayed nominal functioning. Deployment of REM sensors inside of BEAM occurred on June 7, 2016. Six RAMs were deployed one day later. Throughout the remainder of this report BEAM REM sensors will be referred to by chip ID only, i.e. H06 and H10.

This report covers data collection from initial deployment on June 7, 2016 through February 23, 2018, covering 626 days of data. During the initial six months of data collection, was limited by failure of one SSC. SSC 24 failed to power on July 17, 2016 and was off for 11 days. In addition, data collection software was initially not being restarted after the crew logged out of SSC 24. A ground-fix was implemented to auto-start the REM acquisition software as a service. The loss of data has not had a severe impact on assessment of radiation shielding characteristics of BEAM.

Comparison with other ISS REM sensors has been performed using REM D03, deployed in the US LAB, REM G03, deployed in the JAXA JPM, and REM J02, deployed in the Columbus module. During the entire measurement period reported here D03, G03 or J02 were all deployed at a single fixed location. Sensor D03 failed in June of 2017, and G03 failed in November of the same year. However, J02 continued to operate nominally throughout 2018. A picture of H06 deployed at the BEAM port location is shown in figure 1. The sensor is the USB-sized black device shown inside of the red ellipse.

The data download process is shown in figure 2. Data is first captured directly to SSC 24 located in the NOD3 vestibule using the Pixelman software. Data files are transferred autonomously via script on a daily basis to the LS1 Linux server

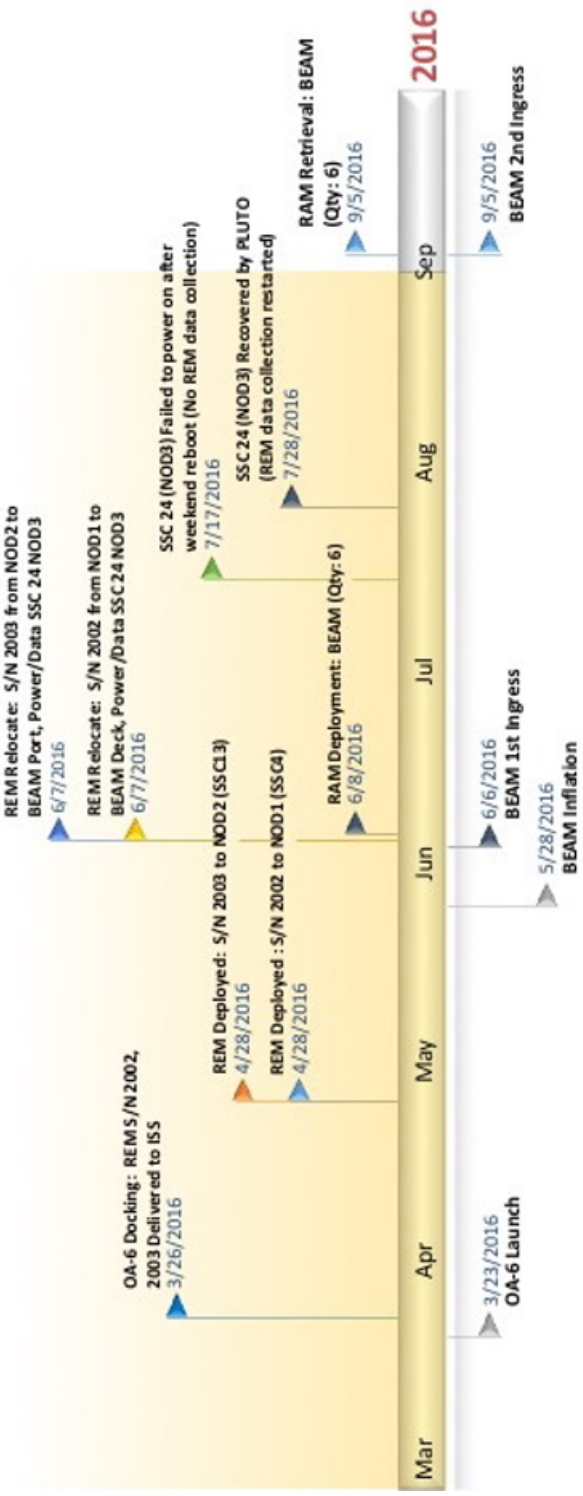

Figure 1. Timeline showing REM sensors H06 (2002) and H10 (2003) launch, deploy and initial measurement period applicable to this report.

located in the US LAB. The script is run once every 9 hours and executed via OCA. Once transferred, raw data files are sent via Ku-band to the ground in White Sands. They are then transferred over to MCC-H and then to the SRAG server for analysis. Data transferred includes raw frame data and log files, including sensor health and status. There is roughly 20 MB of data per day per sensor. This process is identical to that used for all other ISS REM sensors. If configuration files need to be uploaded the process is performed in reverse.

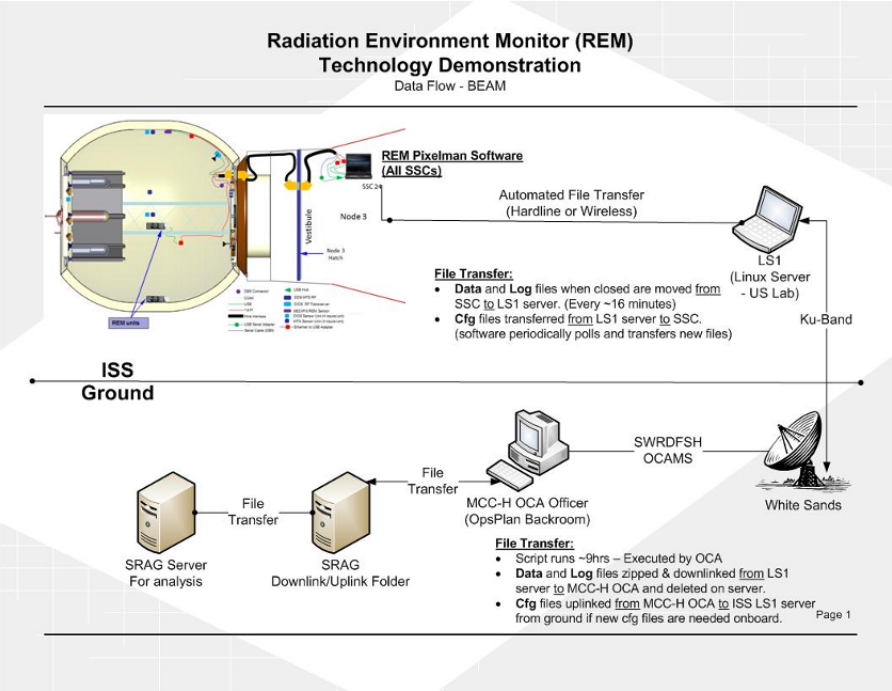

Figure 2. Data flow from sensor to ground for H06 and H10 deployed inside of BEAM.

Three hemispherical shells with differing thicknesses were printed aboard ISS utilizing the Made-In-Space printing facility [4]. Hemispheres of 1.1 mm, 3.3 mm, and 10 mm thickness were printed for deployment over one of the REM units located inside the BEAM module on the port wall centerline in an effort to evaluate the low-energy component of the radiation dose measured by these devices. Table 1 shows the deploy timeline for the shields. Table 2 shows the location of RAMs within the BEAM module. Table 3 shows the corresponding ISS expeditions for RAM measurements inside of BEAM. A listing of all BEAM ingresses is shown in Table 4.

3 Shielding Analysis and Dosimetry Predictions

Predicted daily dose rates have been calculated with the NASA Langley OLTARIS package. Ray-traced CAD models for ISS and BEAM were used as shielding thick-

Table 1. Hemispherical shield deploy timeline.

Item	**Start Date**	**Duration [days]**
BEAM REM Deploy	06/8/2016	–
1.1 mm Shell	04/29/2017	32
3.3 mm Shell	05/31/2017	20
10 mm Shell	06/20/2017	41
10 mm Shell Reorient (Flip)	07/31/2017	207
10 mm Shell Remove	02/23/2018	–

Table 2. Locations of RAMs within BEAM and associated identification labels.

BEAM Location	**46S RAM Identifier**	**48S RAM Identifier**	**50S RAM Identifier**
Next to REM on center of seam next to Quadrant Label "B"	RAM1	RAM5	RAM5
Deck side of Aft bulkhead	RAM2	Cupola_3	RAM6
On center of seam next to Quadrant Label "D"	RAM3	RAM6	RAM1
On center of seam next to Quadrant Label "C"	RAM4	RAM4	RAM4
Next to REM on center of seam next to Quadrant Label "A"	RAM5	RAM3	RAM3
Deck side of Fwd bulkhead	RAM6	RAM 2	RAM2

Table 3. RAM supply flight details.

ISS Expedition	**Soyuz Flight**	**RAM Set**	**Launch/Land Date**	**Days Deployed**	**Altitude [km]**
47/48	TMA-20M	46	03/18/16 - 09/07/16	89.4	403.1
49/50	MS-02 / MS-03	48	10/19/16 - 06/02/17	218.9	404.7
51/52	MS-04 / MS-05	50	04/20/17 - 12/14/17	206.9	404.5

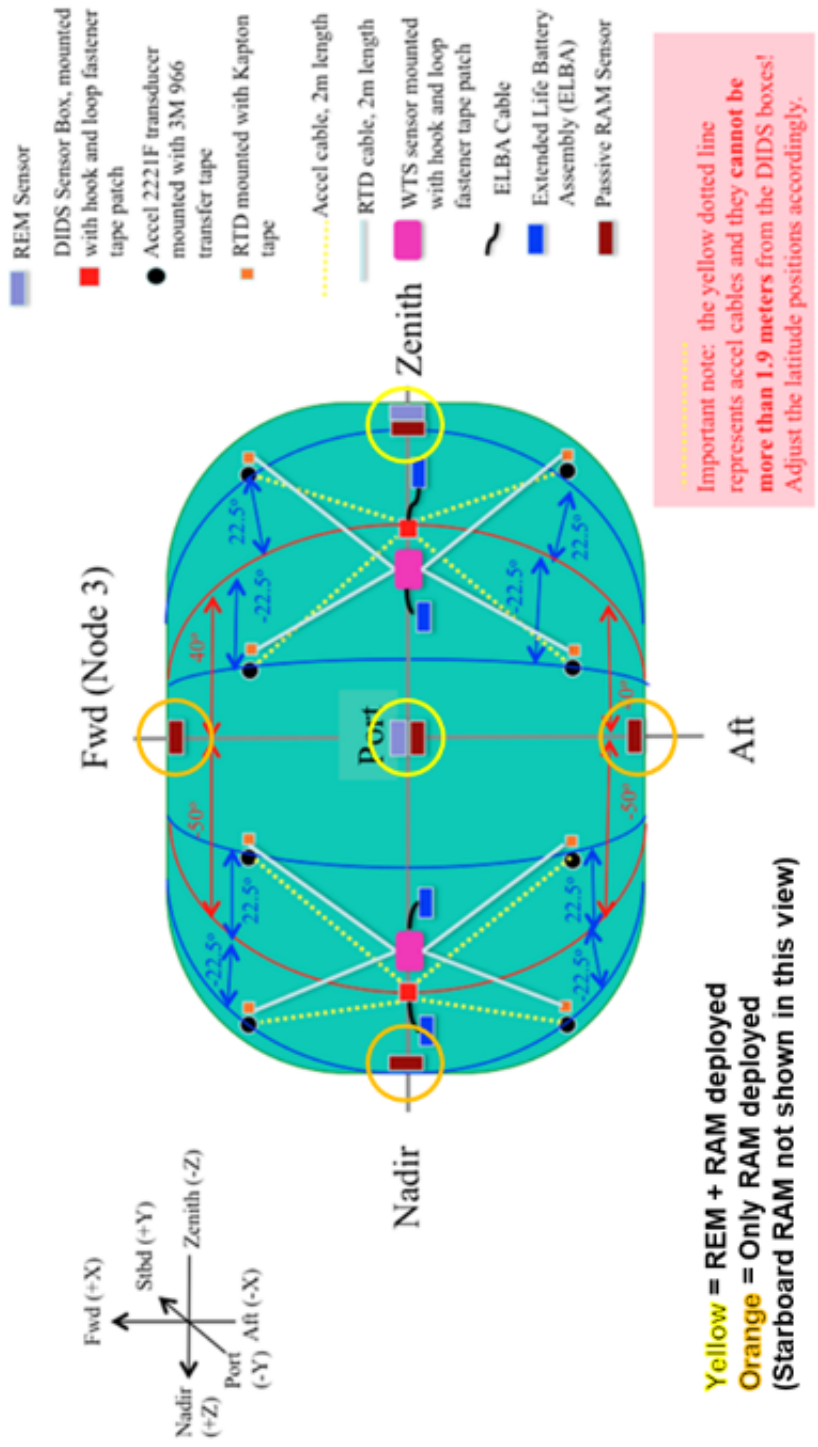

Figure 3. REM and RAM placement within the BEAM module.

Table 4. BEAM Ingress (hatch open) activities from 2016 through August 2019

Year	Day	Time	Date	Epoch Time
2016	159	08:20	06/07/2016	1465287600
2016	160	08:20	06/08/2016	1465374000
2016	249	11:30	09/05/2016	1473075000
2016	249	12:25	09/05/2016	1473078300
2016	273	12:35	09/29/2016	1475152500
2016	298	09:25	10/24/2016	1477301100
2017	033	12:50	02/02/2017	1486039800
2017	081	10:40	03/22/2017	1490179200
2017	118	12:25	04/28/2017	1493382300
2017	151	11:50	05/31/2017	1496231400
2017	171	09:10	06/20/2017	1497949800
2017	212	09:00	07/31/2017	1501491600
2017	234	13:50	08/22/2017	1503409800
2017	324	09:55	11/20/2017	1511171700
2017	325	10:25	11/21/2017	1511259900
2018	053	14:20	02/22/2018	1519309200
2018	138	10:00	05/18/2018	1526637600
2018	214	14:50	08/02/2018	1533221400
2018	228	12:05	08/16/2018	1534421100
2018	268	10:20	09/25/2018	1537870800
2019	023	08:15	01/23/2019	1548231300
2019	113	08:05	04/23/2019	1556006700
2019	157	08:15	06/06/2019	1559808900

ness input. All rays for BEAM were taken to be equivalent aluminum thicknesses. For ISS, both aluminum and polyethylene equivalent thicknesses were used. The newest version of the BON GCR model is not currently available in OLTARIS and thus input GCR flux spectra were modeled from the 2003 at a point of comparable solar activity as measured by sunspot number and F10.7 solar radio flux.

Shielding ray distributions are shown in figure 4. Distributions of ray thicknesses is produced by raytracing each CAD model. A raytrace has been done for each REM sensor configuration. Additional traces were performed on the ISS model without BEAM attached and with BEAM isolated from ISS. Each trace is done by selecting a point through which all rays are then drawn. There are a total of 104 rays evenly spaced over 4π for each raytrace. The top plot shows the fraction of rays exceeding a given equivalent aluminum thickness versus equivalent aluminum thickness in g/cm^2. As expected, the ISS distribution is quite broad with thicknesses out to roughly 800 g/cm^2.

Histograms of each ray distribution (except for BEAM REM port location – similar to BEAM REM deck) are shown in the bottom plots. The ray trace of the BEAM model not attached to ISS about the BEAM center point has a much higher number of thicknesses below 10 g/cm^2, with a pronounced peak at 4.5 g/cm^2. This peak corresponds to the equivalent aluminum thickness of the pressure shell, derived from the actual BEAM material composition and thicknesses. There are in addition a number of lower thickness rays, determined to be from rays that pass through thin sections at interface points in the BEAM hatch. This is likely only an artifact of the CAD model itself. However, the addition of ISS to the final shielding distribution removes many of these small-thickness rays.

The largest difference in shielding distributions between BEAM attached to the ISS using a BEAM ray center point versus a ray center point in the US LAB is over a range of thicknesses from 5 to 40 g/cm^2 with the US LAB thicker by roughly a factor of 2.5. Comparison of the bottom third and fourth plots shows that the US LAB center point distribution and that centered on the BEAM REM deck location are quite similar in both range of thicknesses and spectral form. For this reason it may not be surprising that GCR trends pre- and post-deployment are similar.

Calculated average daily dose rate results are shown in Table 1. Predicted GCR daily dose rates are essentially constant regardless of whether or not BEAM is isolated from ISS or modeled attached to it. The difference in modelled daily dose from GCR between the BEAM-only model and the US LAB CHeCS rack is 3 – 5%. Interestingly, these same values are found when using the full ISS/BEAM model. Such a small variation is well within the statistical error of the model calculation and thus the only statistically meaningful conclusion is that there is no observed difference in GCR daily dose. This is in rough agreement with measurements if one takes into account an approximately $\pm 10\%$ systematic error in the REM data, i.e. relative change in GCR daily dose rate pre- and post-deployment ranges from 4% to 8%.

Trapped dose rate ratios (last column in Table 5) range from 2.44 to 4.17 over all different configurations calculated. With BEAM modeled attached to ISS (measurement configuration) the range is 2.44 to 3.03. The measured shift in dose rate for both H06 and H10 sensors between pre- and post-deployment inside of BEAM is

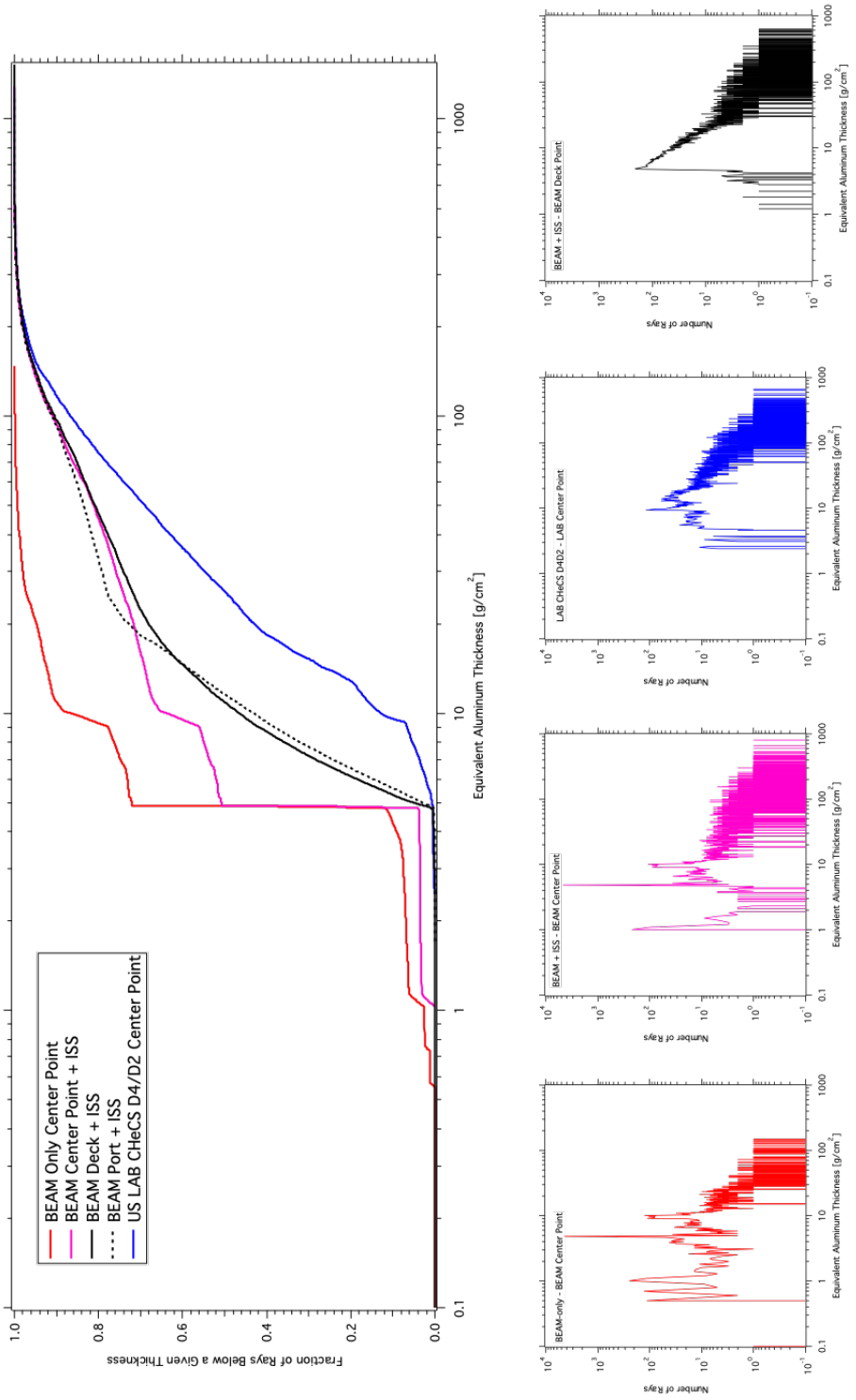

Figure 4. Distribution of ray lengths as an equivalent aluminum thickness in g/cm^2 for different point locations.

roughly a factor of 3. It has already been discussed that the increase in daily dose rate appears to be dominated by increase in SAA (trapped field) dose rate. The modeled BEAM deck and port ratios where H06 and H10 are deployed is 2.46 and 2.44 respectively, 24% lower than the measured ratio. This may be due to how BEAM is modeled. The as-used CAD model represents all sections of the pressure shell, except for the end caps, as equivalent aluminum with a thickness of 4.5 g/cm^2 and thus neglects the layered nature and MMOD shielding details. To assess the impact on daily dose rate future calculations will be performed on simulated 'slabs' of material that more closely resemble the true composition of the BEAM pressure shell.

Total dose values predicted at the BEAM deck and port locations underestimate the measurements by nearly a factor of five. OLTARIS utilizes the 2010 version of HZETRN. The decision to start with the OLTARIS framework was based upon ease of result generation. In addition, the team decided to run several different versions of HZETRN to enable a cross comparison of potential differences. Preliminary results using the 2015 version are ready for analysis but could not be prepared in time for this report. These results will be included in the next BEAM report. These first results however show predictions of total dose that are much more in line with measurements.

Table 5. Predicted daily dose rates using the OLTARIS package and ISS and BEAM CAD models.

	GCR Dose$_{Si}$ [μGy/day]	**Trapped Dose$_{Si}$ [μGy/day]**	**Total Dose$_{Si}$ [μGy/day]**	**Ratio To US LAB CHeCS Rack (GCR, Trapped Total)**
Beam-Only Model				
BEAM Center	40	217	257	1.02, 4.17, 2.82
BEAM Deck REM	41	162	203	1.05, 3.11, 2.23
BEAM Port REM	41	167	208	1.05, 3.21, 2.28
ISS/BEAM Model				
BEAM Center	40	158	198	1.02, 3.03, 2.17
BEAM Deck REM	41	128	169	1.05, 2.46, 1.85
BEAM Port REM	41	127	168	1.05, 2.44, 1.84
ISS Reference				
US LAB CHeCS Rack	39	52	91	1

Predicted daily dose rates have been calculated using HZETRN2015 coupled with mass shielding estimates from ISS CAD models and supplied BEAM specifications. In the first report the OLTARIS package was used a different environmental definition for the trapped and GCR environments. All rays in the shielding estimate calculations for BEAM were taken to be equivalent aluminum thicknesses. For ISS, both aluminum and polyethylene equivalent thicknesses were used. The flight dates

Table 6. Predicted daily dose rates for RAM dose point locations using the following conditions: Start Date - 07/01/2013; End Date - 09/01/2013; Total Days - 62; ISS Altitude - 410 km; Orbit - circular.

Location	**GCR Dose$_{Si}$ [μGy/day]**	**Trapped Dose$_{Si}$ [μGy/day]**	**Total Dose$_{Si}$ [μGy/day]**
Beam-Only Model			
Fwd RAM	55	769	824
Aft RAM	56	705	761
Port RAM	55	688	742
Stbd RAM	55	683	738
Ovhd RAM	55	686	740
Deck RAM	55	688	743
ISS/BEAM Model			
Fwd RAM	68	417	484
Aft RAM	62	533	595
Port RAM	61	524	585
Stbd RAM	63	475	539
Ovhd RAM	62	526	588
Deck RAM	62	539	600
ISS Reference			
US LAB CHeCS Rack	70	212	282

are not available in the current version of the BON 2014 GCR model, thus input GCR flux spectra were modeled from 2013 at a point of comparable solar activity as measured by sunspot number and F10.7 solar radio flux.

Calculated average daily dose rate results are shown in Table 5 and 6 for REM and RAM locations using HZETRN2015 and ISS/BEAM CAD models as described previously. Predicted GCR daily dose rates are essentially constant regardless of whether or not BEAM is isolated from ISS or modeled attached to it. The difference in modeled daily dose from GCR between the BEAM-only model and the US LAB CHeCS rack is around 20%. Values of 3-12% are found when using the full ISS/BEAM model. This is in rough agreement with measurements if one takes into account an approximately +/- 10% systematic error in the REM data, i.e. relative change in GCR daily dose rate pre- and post-deployment ranges from 4% to 8%.

Trapped dose rate ratios (last column in Table 5) range from 2.46 to 4.33 over all different configurations calculated. With BEAM modeled attached to ISS (measurement configuration) the range is 2.46 to 3.12. The measured shift in dose rate for both H06 and H10 sensors between pre- and post-deployment inside of BEAM is roughly a factor of 3. It has already been discussed that the increase in daily dose rate appears to be dominated by increase in SAA (trapped field) dose rate.

The modeled BEAM deck and port ratios where H06 and H10 are deployed is 2.50 and 2.46 respectively, 16% lower than the measured ratio. This may be due to how BEAM is modeled, in conjunction with the transport and external environment definition. The as-used CAD model represents all sections of the pressure shell, except for the end caps, as equivalent aluminum with a thickness of 4.5 g/cm^2 and thus neglects the layered nature and MMOD shielding details. To assess the impact on daily dose rate future calculations will be performed on simulated 'slabs' of material that more closely resemble the true composition of the BEAM pressure shell.

In the aluminum equivalent shielding information shown in Figure 4, the shell deploy affects approximately half of the 10,000 rays in the modeled shielding distribution and increases the areal density of shielding in the positive or negative x-plane (Phi), depending on shield orientation, by roughly 0.06 g/cm^2, 0.17 g/cm^2, and 0.5 g/cm^2 of aluminum equivalent for the 1.1 mm, 3.3 mm, and 10 mm hemisphere thicknesses, respectively.

4 Results and Discussion

4.1 Absorbed Dose / Dose Rate Trends - BEAM Empty

4.1.1 Active REM Absorbed Dose Measurements

Daily dose rate in H_2O for H06, H10, D03 and ISS TEPC as a function of time is shown in Figure 5. The point is time denoting deployment of H06 and H10 inside of BEAM is denoted by the vertical solid line. Dose rate for the REM sensors is natively calculated in silicon. For comparison to ISS TEPC measurements REM dose rate has been converted to dose in H_2O by using the ratio of stopping powers. Data is shown for roughly one month before deploy inside of beam and two months

after deploy.

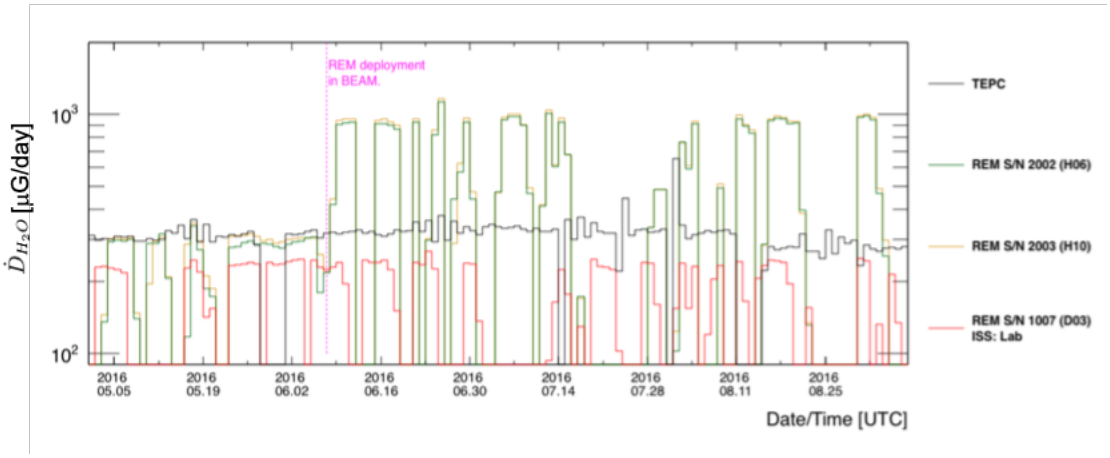

Figure 5. Daily dose rate in water for H06, H10, D03 (located in the US LAB) and the ISS TEPC (located in the SM). The vertical line marks the point in time where H06 and H10 were relocated from ISS to inside of BEAM. Prior to deployment inside of BEAM both H06 and H10 tracked well with ISS TEPC.

Before deployment both H06 and H10 daily dose rates were comparable to ISS TEPC values. D03 trends approximately 30% lower than H06, H10 and TEPC pre-deployment and maintains nearly the same daily dose rate throughout the measurement period. This constant lower dose rate compared to ISS TEPC is indicative of shielding differences between the US LAB and NOD1 and NOD2.

Deployment inside of BEAM shows dose rates as measured by H06 and H10 increasing roughly a factor of 3 above the pre-deployment values. Note also that both sensor track very close to each other in magnitude. Gaps in the data are caused by closing of the data acquisition software on SSC 24 once the crew logs out of the laptop. As mentioned above a fix to ensure greater data capture is being worked.

The ratio in dose rates between H06 and D03, and H10 and D03 as a function of time is shown in Figure 6. The vertical line marks the point in time where REM sensors were deployed inside BEAM. The horizontal green, purple and black lines are only to guide the eye to regions of relatively constant dose rate in time. Shown are dose rates separated by data coming from either the SAA or GCR at high latitudes. Pre-deployment SAA ratios are found to be ¡1, indicating that H06 (NOD1 location) and H10 (NOD2 location) measured dose rates are higher than D03 (US LAB location). It is known that the US LAB is one of the most heavily shielded locations on ISS and thus lower dose rates are not surprising. Once deployed the SAA ratios decrease by roughly a factor of three indicating yet higher dose rates inside of BEAM compared to the US LAB. Inside of BEAM both H06 and H10 dose rates differ by only a few hundredths of a μGy/day. This is the reason the black down triangles are not visible in the plot after deployment.

GCR ratios show a different behavior than those for the SAA (Figure 6). Both pre- and post-deployment ratios are > 1, indicating that GCR dose rates are higher

in NOD1 and NOD2 than in the US LAB. Approximately 1 week after deployment inside of BEAM GCR ratios appear to increase, indicating that GCR dose inside of BEAM is lower than the US LAB. The shift is not constant but transient in time, decreasing nearly back to pre-deployment values over about a three-week time period. The cause for this behavior is being investigated.

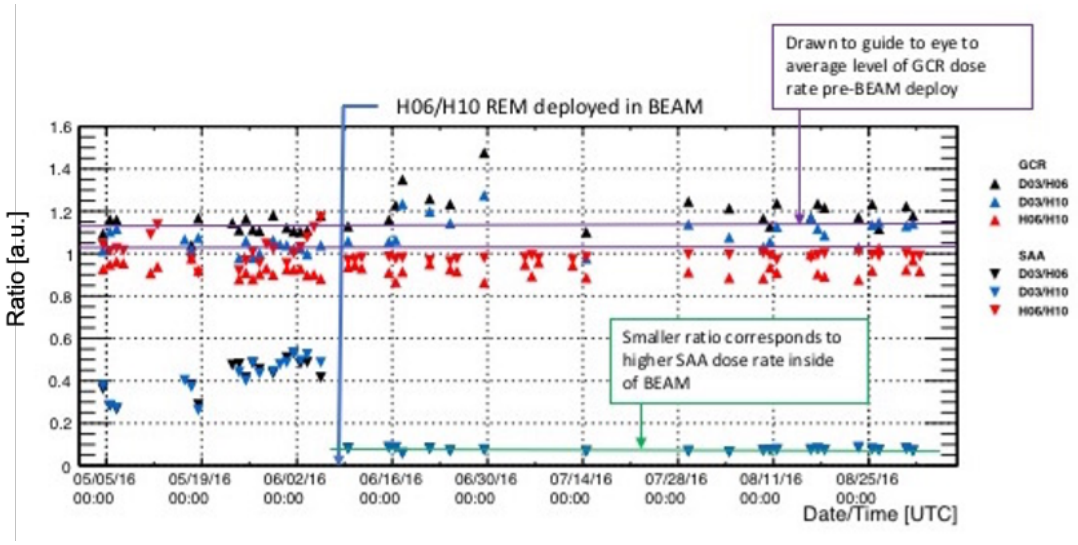

Figure 6. Dose rate ratio of H06 and H10 to REM sensor D03 located in the US LAB. All three horizontal lines are drawn just as reference to guide the eye. The vertical line marks the point in time of REM deployment inside of BEAM.

Ratios averaged over the first few months are shown in figure 6. Results comparing H06 and H10 measurements to D03 in the US LAB are similar to results shown in Figure 6. However, also shown are ratios with respect to G03 located in the JAXA JPM and J02 located in the Columbus module. What is clear in the figure is that the magnitude of the shift post BEAM deployment is highly dependent on sensor location in other ISS modules. Ratios indicate that G03 shows, on average, a higher SAA dose rate than both H06 and H10 before deployment but a lower average dose rate after deployment. J02 shows a lower average dose rate both pre- and post-deployment. Trends in average GCR dose rate across all sensor ratios are similar to what is seen in Figure 6. In all cases there appears to be a shift to slightly (¡= 8%) lower average GCR dose rates once H06 and H10 are deployed inside of BEAM. Although this trend is consistent across all sensors the magnitude of the shift is within the estimated systematic measurement uncertainty of $\pm$ 10%. More measurement time and analysis is needed to assess whether or not this shift is real.

Long-time daily dose rate covering pre-deploy through the end of the technology demonstration with BEAM empty is shown in Figure 8. Note that coverage for D03 and G03 over this two-year period is limited. The time of sensor deploy inside of BEAM is denoted by the black vertical line in the top plot. The total daily dose rate

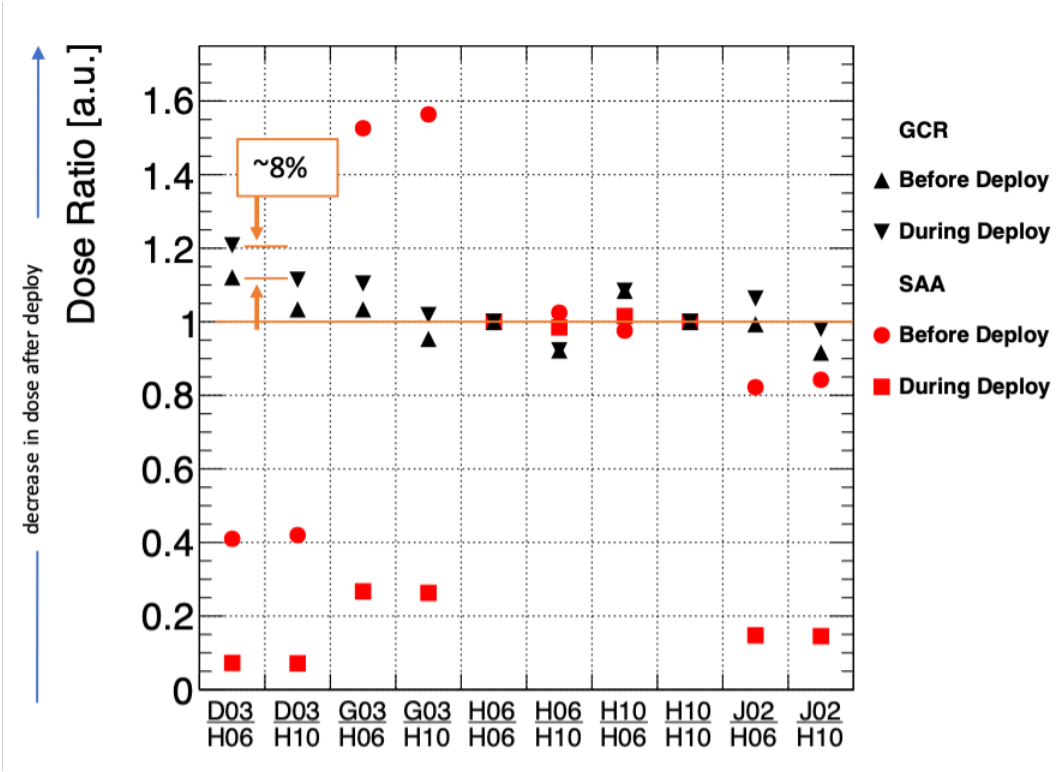

Figure 7. Ratio of dose rates for H06 and H10 relative to REM sensors D03 (US LAB), G03 (JAXA JPM) and J03 (Columbus). Higher ratios correspond to lower measured dose rates after deploy inside of BEAM and lower ratios to higher measured dose rates after deploy. The orange horizontal line is to guide the eye at a ratio of 1. Note the large variability in ratio depending on which REM sensor (D03, G03, J02) is used. This is likely reflective of variability in ISS shielding distribution from module to module across ISS. In all cases however the ratio drops after deploy to BEAM indicating a higher dose rate regardless of which ISS module is used for comparison.

for each sensor has been delineated into three additional components by performing cuts along iso-lines in daily dose rate, L-shell values and magnetic field magnitude (IGRF). The L-shell value characterizes the grouping of geomagnetic field lines that cross Earth's equator at a given radial distance, express in terms of Earth radii. The total daily dose is simply the summed dose rate values for the entire day. The SAA is defined by ? Polar dose rate is defined as the 0.12 μGy/hr isoline not contained in the SAA. GCR daily dose rate is everything remaining.

It is clear from the figure that both the H06 and H10 sensors show a large jump to greater total and SAA daily dose when moved from heavier shielded locations inside of ISS to the inside of the BEAM module. For both BEAM sensors, however, the GCR daily dose shows a drop by approximately 26%. These trends persist throughout the remaining two-year measurement time. Note the spikes in polar daily dose rate in the September, 2017 time frame. This coincides with the occurrence of a Solar Proton Event (SPE) which will be discussed in detail in Section 4.3. It is not surprising that the signal is strongest in the polar regions since it is precisely the location where one expects streaming of energetic particles to be able to penetrate the geomagnetic field down to ISS altitudes.

World maps showing dose rates in H2O (ISS TEPC) and silicon (REM) along the ISS ground track are shown in Figure 9. The red circle in each plot is drawn to guide the eye to latitude/longitude regions where differences have been observed between sensors deployed in BEAM and other ISS modules. For comparison ISS TEPC dose rates where plotted for time periods before and after REM sensor deployment (Figure 9 (a) and (b), respectively). Measured dose rates were essentially unchanged across the entire pre- and post-deployment periods, as expected since TEPC did not move locations. If a change would have been observed it could only be due to changes in the environment, e.g. Space Weather and/or changes in ISS altitude. Regions of relatively larger dose rates is observed at the upper latitudes (east of Africa and over North America) and within the SAA. The latitudinal and longitudinal extent of increased dose rate over the SAA is consistent with historical trends, spanning roughly from -70^o to -10^o in longitude and -45^o to 0^o in latitude.

Figure 9 (c) and (d) show dose rates in silicon for REM sensor H06 before and after deployment inside of BEAM, respectively. Recall that before deployment H06 was located in NOD1 and showed daily dose rates comparable to the ISS TEPC. The 2d intensity map also looks similar between H06 and TEPC before deploy. After deployment the dose rate map for H06 (Figure 9 (d)) shows a difference in the mapping of the SAA. Most notably is the higher dose rate in the SAA out to roughly 20^o longitude and -50^o latitude. Although not nearly as clear, the upper latitude dose rates appear higher as well after deployment. This same trend appears in the H10 measurements (Figure 9 (e) and (f). World maps for the D03 sensor, located in the US LAB throughout the entire reporting period, are show in Figure 9 (g) and (h). As expected, distributions in dose rate over the ISS ground track look nearly identical for the pre- and post-deploy data collection periods.

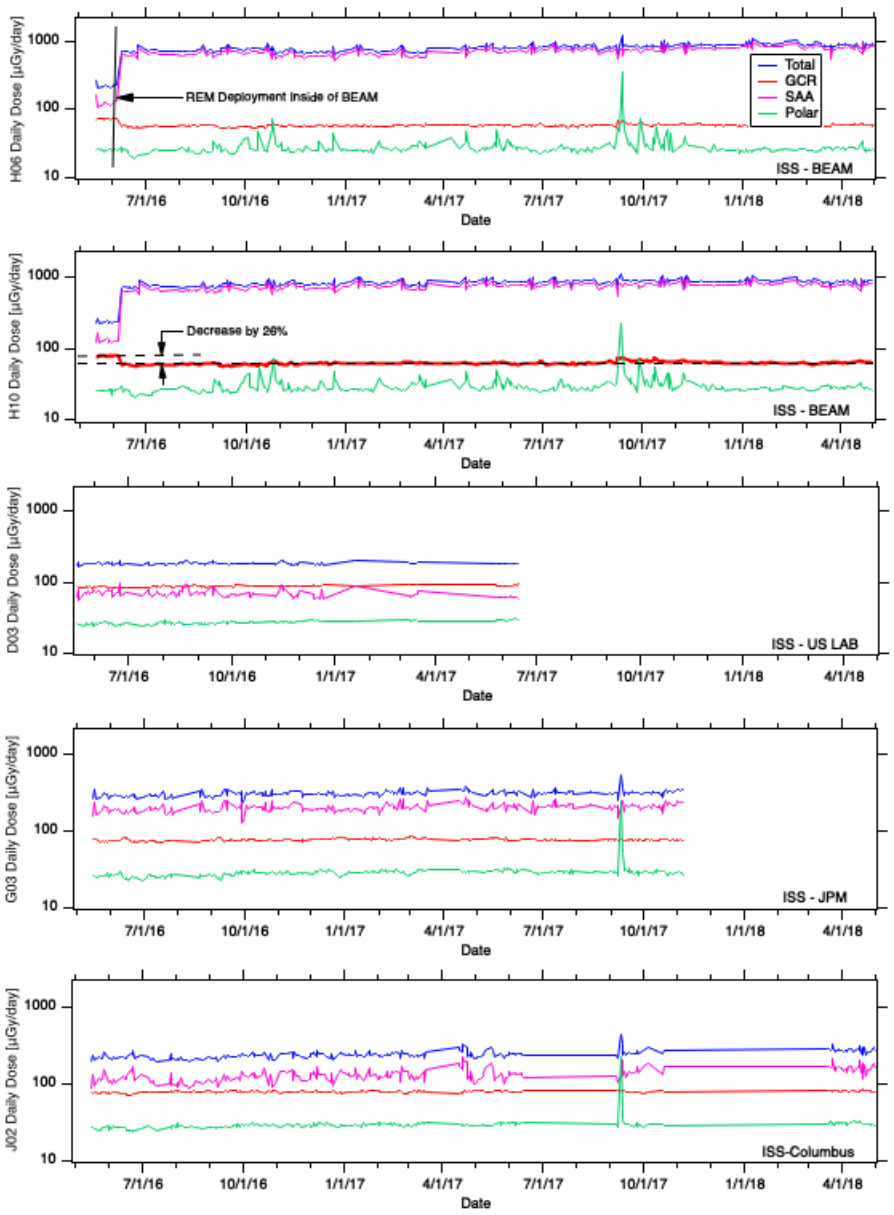

Figure 8. Daily dose rate for H06, H10, D03 (located in the ISS US LAB), G03 (located in the ISS JPM) and J02 (located in the ISS Columbus module). Daily doses are shown only for days where the REM unit was on and acquiring data for $\geq 95\%$ of the time. The black vertical line on the left side of the top plot marks the point in time where the H10 and H06 sensors were moved from the ISS NOD2 and NOD1, respectively, to the inside of BEAM.

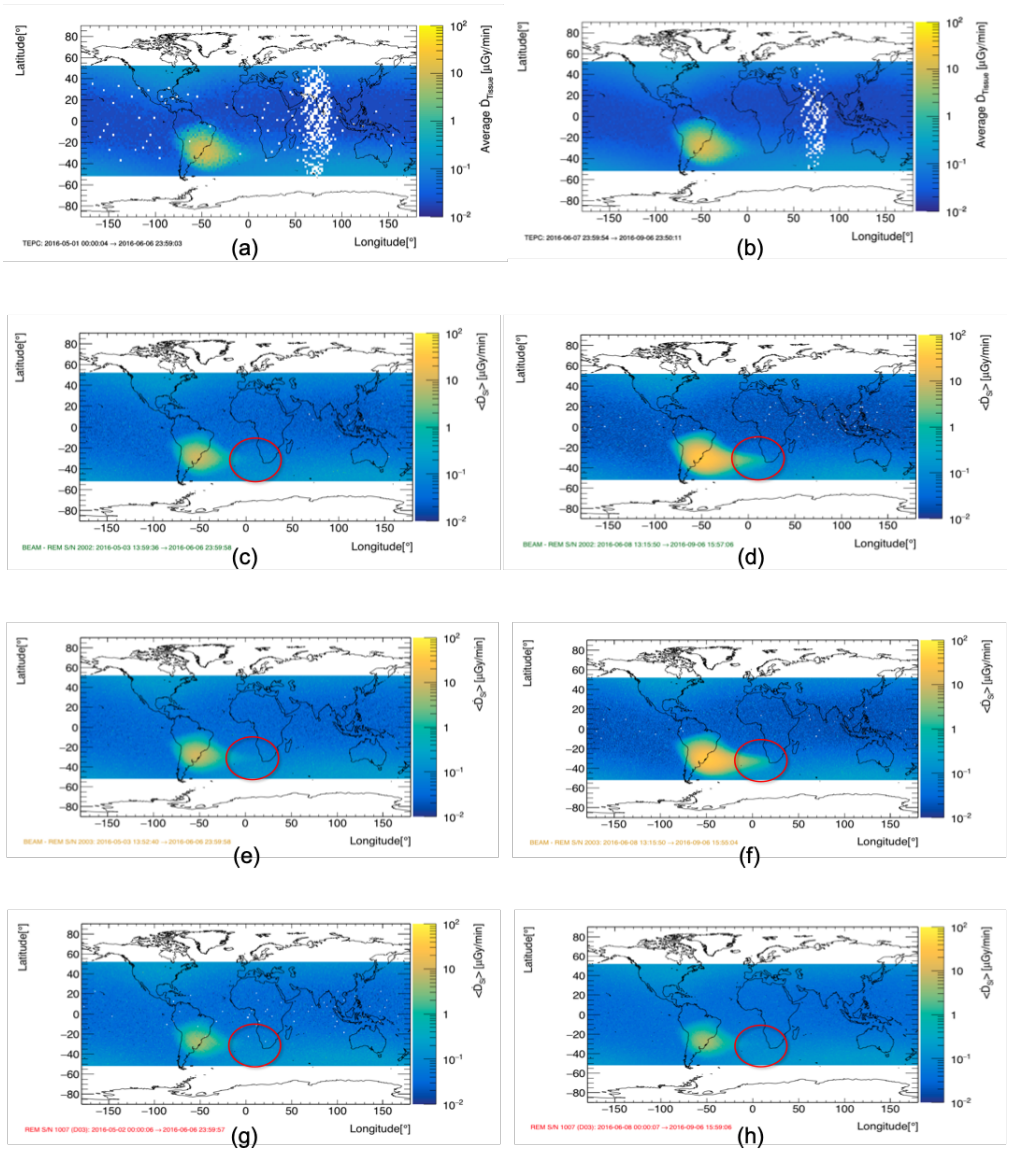

Figure 9. Dose rate maps showing the SAA intensity both before BEAM REM deployment (left column) and after (right column) for the following detectors: ISS TEPC before (a) and after (b); BEAM REM H06 before (c) and after (d); BEAM REM H10 before (e) and after (f); ISS LAB REM D03 before (g) and after (h).

4.1.2 Passive Radiation Area Monitor (RAM) Absorbed Dose Measurements

Three sets of six passive RAMs were flown to ISS in support of the BEAM radiation measurements (see Table 2). The BEAM RAMs have been processed post-flight in the Space Radiation Dosimetry Laboratory (SRDL) at JSC.

The RAMs were placed at six different locations inside BEAM as shown in Figure 3. The yellow circles show the position of RAM collocate with REM, while the orange circles show the other four RAM positions. Since the RAMs have not been placed in the same locations from mission to mission, Table 3 shows the specific BEAM locations and associated RAM identification labels for all three ISS missions.

A summary of the daily dose rates for the six RAMs are shown in Figure 10. The maximum dose rate measured by the RAMs corresponded to the RAM located next to the Radiation Environment Monitor (REM) on center of seam next to Quadrant Label "B", with values ranging from 880.4 ±20.11 μGy/day (48S) to 1003 ±21.28 μGy/day (50S). The minimum RAM dose rates were usually measured in the Deck side of Aft bulkhead location with values ranging from 676.6 ±15.76 µGy/day (48S) to 735.3 ±14.53 μGy/day (50S).

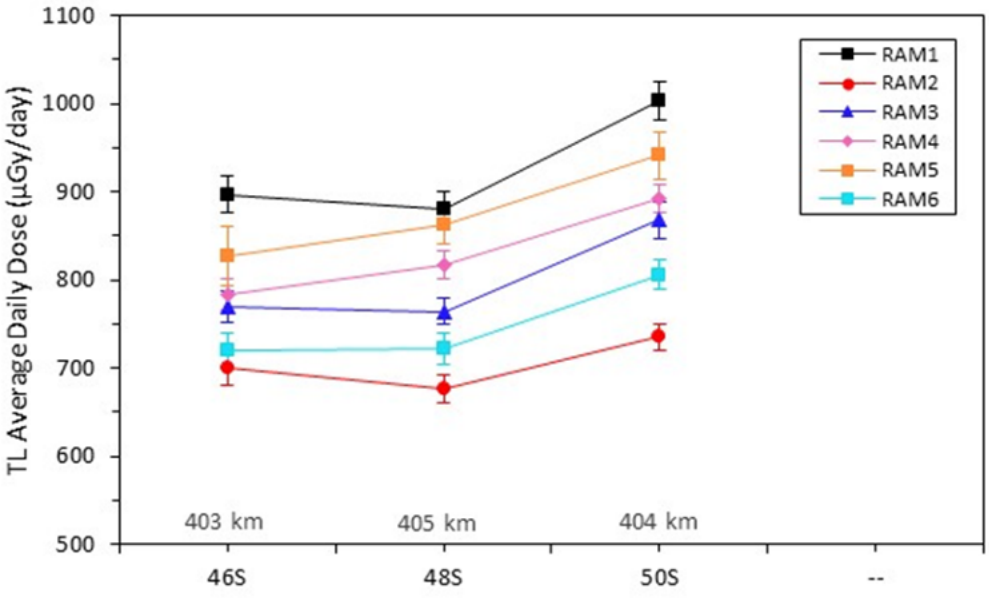

Figure 10. Summary of 46S BEAM RAM data (06/08/2016 – 11/21/2017).

Figure 11 shows a comparison between the RAM daily dose rate data and two US Lab locations inside ISS. The RAM located at LAB1_D3 reads usually the highest within the US Lab since it is placed in the proximity of the low-shielded US Lab window. The RAM placed inside the CHeCS Rack is representative for the minimum dose inside the US Lab. Data comparison shows BEAM RAMs dose rate values up to 2X higher than the maximum US Lab dose rate. This is consistent with the

increase of roughly a factor of three observed in daily dose as measured with the REM sensors. Two of the BEAM RAMs have been collocated (i.e., placed on the

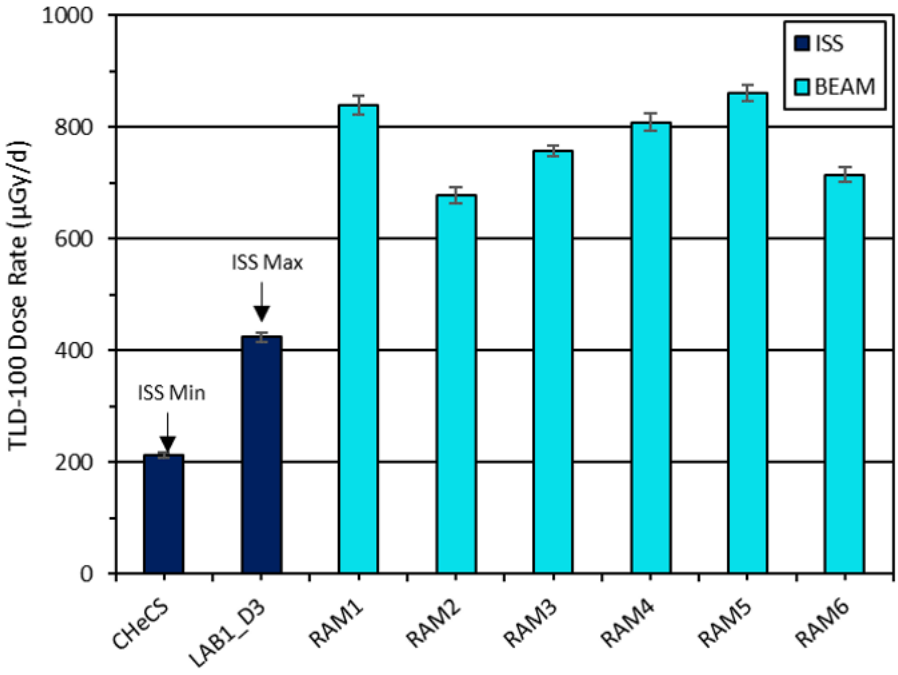

Figure 11. 48S BEAM RAM data comparison with ISS Min and Max (10/19/2016 – 06/02/2017).

wall in close proximity) with the REM units (H06 and H10). Figure 12 and Figure 13 show a comparison between the passive detectors and the active instruments during 50S.

The active REM S/N 2003 (H06) dose to water values for all three mission increments ranged from 4-13% from the RAM passive detectors measured doses, while the active REM S/N 2002 (H10) dose to water values ranged from 3-20% from the RAM passive detectors measured doses. The increase in the REM/RAM difference with time is primarily attributed to the REM location change during 50S vs. 46S (see Figure 6). Figure 14 includes the REM active units' response during the shell deploy.

4.2 Hemispherical Shield Spectral Analysis

To ultimately determine whether or not a modest amount of passive shielding is sufficient to attenuate the increase in dose rate one needs to know the energy of the particles and particle type. What is needed is energy spectra of electrons, protons and heavier ions from 1 MeV out to 1 GeV. This is difficult at best. Instead, we have pulled on external data via the ISS EV-CPDS, JAXA/SDOM instrument and reconstructed energy spectra from BEAM REM data, allowing us to determine the

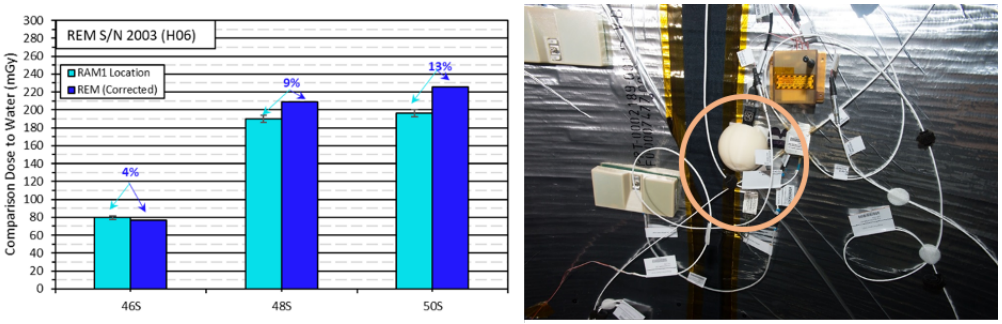

Figure 12. Mission dose comparison of REM SN 2003 (H06) with attached RAM1 (06/08/2016 – 11/21/2017) The RAM is visible below the REM with shield shell deployed.

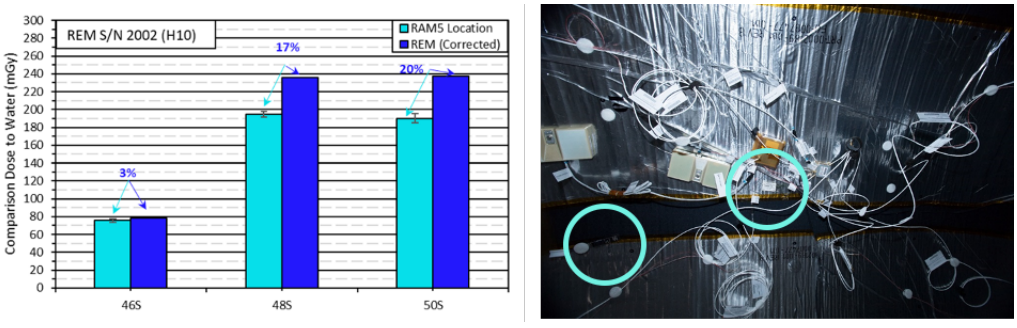

Figure 13. Mission dose comparison of REM SN 2002 (H10) with attached RAM5 (06/08/2016 – 11/21/2017). The REM is to the bottom left, with the RAM located near picture center.

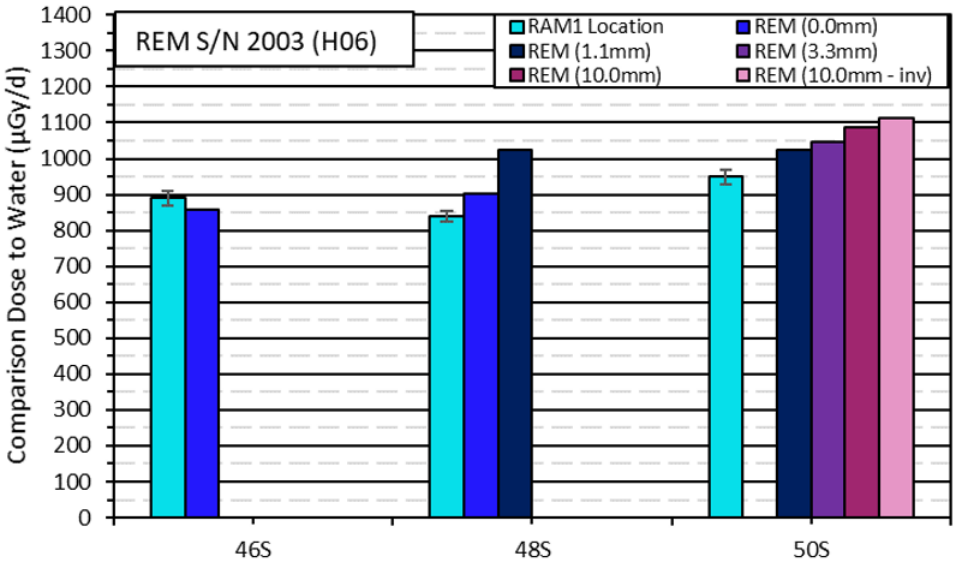

Figure 14. Comparison of REM SN 2003 (H06) daily dose with attached RAM dose (BEAM/RAM1) (06/08/2016 – 11/21/2017). REM covered by 1.1 mm PE shield from 04/28/2017 - 05/31/2017; 3.3 mm PE shield from 5/31/2017 – 06/20/2017; 10.0 mm PE shield from 06/20/2017 – 07/31/2017; inverted 10.0 mm PE shield from 07/31/2017 – 11/21/2017 (RAM retrieval).

likely particle type and energy range contributing to the increase in dose rate.

The internal spectra generation using REM data is still in work. However, we expect the low energy component to be the most accurate. JAXA/SDOM differential energy spectra show high populations of electrons out to roughly 21 MeV, the upper energy limit of the instrument. Energetic electrons are also observed in the SAA with the same instrument over an energy range of 8 to 21 MeV. The modeled equivalent aluminum thickness of the combined ISS-BEAM structure is peaked at 1.66 cm. However, 50% of the rays sampled from the CAD model of BEAM attached to ISS have equivalent aluminum thicknesses greater than or equal to 4.2 cm. The range in aluminum of the most energetic SDOM electrons measured is only about 4 cm. Thus, a large fraction of the combined ISS-BEAM structure will shield against these electrons. Moreover, electrons up to roughly 8 MeV appear in the SDOM measurements at upper and lower latitudes yet the dose as a function of latitude and longitude does not show an increase over pre-BEAM measurements in these regions, implying that energetic electrons are not contributing in any substantial manner to the observed increase in daily dose. It's important to note here that although the majority of the BEAM structure is not aluminum it is a common radiation shielding practice to convert non-metallic structures to equivalent aluminum thickness for comparison.

Figure 15 shows a typical EV-CPDS dose rate intensity plot as a function of ISS latitude and longitude (bottom graph). The top graph shows daily dose intensity inside of BEAM with the H10 REM sensor. Note that the magnitude of dose rates cannot be compared here. EV data is telemetered dose rate in mrad/min. For the REM data, it was decided to focus on dose per day. Comparison of the shape and extent in latitude and longitude however should be valid.

What is interesting here is the similarity with the measured dose rate inside of BEAM, particularly the region of the SAA. It appears that the external environment shows both a larger SAA region as well as greater extent to more negative latitudes and positive longitude than measurements inside of the US LAB. Qualitatively the shape is similar to what has been observed inside BEAM. Moreover, the increase in extent to positive longitude and lower latitude is nearly identical between the two measurements. This supports the notion that sensors inside of BEAM are sampling parts of the external environment that are typically shielded for other ISS modules. Since the BEAM shielding distribution is peaked at lower thickness than for instance a point in the US LAB we expect the similarity between REM measurements and EV-CPDS to be due to lower energy particles.

An external proton spectrum measured with the JAXA SDOM instrument for a single day during BEAM REM measurements (06/13/2016) is shown in Figure 16 (right graph). SDOM data was chosen here for the particular reason that it was calibrated to measure differential proton flux as a function of proton energy and thus allows one to assess the relative difference in flux between low and higher proton energies. The observed spectrum is, as expected, nearly monotonically decreasing as a function of increasing energy. Lower energy flux (¡20 MeV) extends up to more than 2 orders of magnitude higher than protons with energy ¿20 MeV.

Figure 17 shows the constructed proton energy spectrum from the H06 REM sensor. The inset shows the entire constructed spectrum out to 900 MeV. The

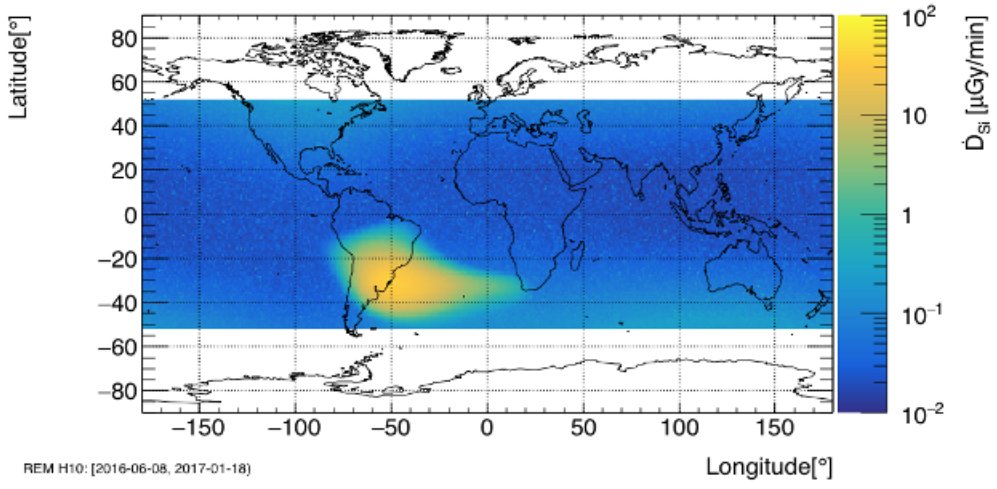

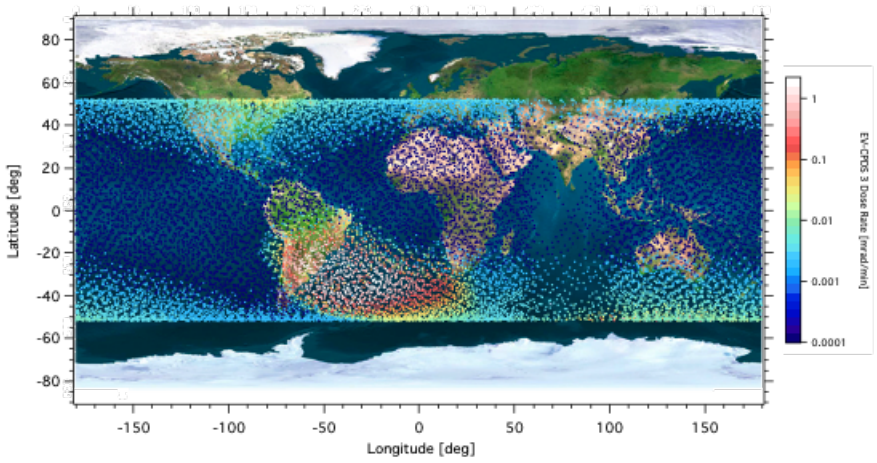

Figure 15. Comparison of BEAM REM dose rate (top) and dose rate measured by EV-CPDS outside of ISS (bottom). EV data is a one-minute telemetered rate which is lower than daily rates.

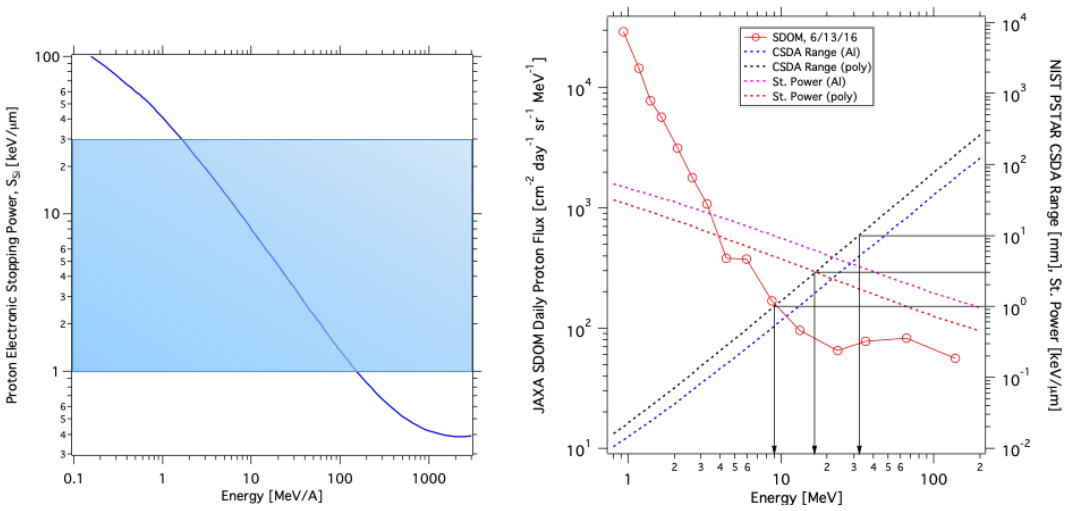

Figure 16. (Left) Proton electronic stopping power in silicon as a function of proton energy. (Right) JAXA/SDOM daily proton differential flux for 06/13/2016. Also shown is the proton electronic stopping power in aluminum and polyethylene and the proton range in both of these materials. The horizontal and vertical black lines mark the proposed shielding thickness and corresponding cutoff energy. The blue shaded region (Left) denotes the LET region of interest where the measured REM differential LET spectrum shows an increase.

blue circles/line are from data taken before deployment inside of BEAM. The pink connected circles/line are from data during BEAM deploy. It is quite clear from this figure that the relatively large difference between these two spectra is for particles of 5 to 70 MeV in energy, supporting the conjecture that lower energy protons are the cause of the increase in daily dose. Note that this does not translate directly to the external proton spectrum since the protons measured by H06 inside of BEAM have been down-modulated in energy by the BEAM pressure shell.

External proton and electron spectra external to both ISS and BEAM are limited in terms of energy range. AMS data, with a low-energy cutoff of several hundred MeV, would provide insight into the higher energy component of the trapped proton environment. This will be investigated in the future. However, being that all of the trends observed in LET changes, latitude and longitude dose rate variation, and reconstructed energy spectra differences between pre-BEAM and BEAM measurements point to a greater dose contribution from particles less than 100 MeV there is no reason at this time to expect deviations at higher energies to be present. One way this could be teased out further is through the use of additional shielding. One must also delineate here between low-energy particles in the external environment and those from attenuation and energy modulation of the incident field by the BEAM-ISS structure.

One possible method to tease out the relative contribution to increased dose rate is to utilize several different thicknesses of passive shielding placed directly over

(around) the REM sensors inside of BEAM, and look for changes in the dose rate and proton energy spectrum. The thicknesses available would not shield out high-energy protons but would allow one to assess whether or not the low-energy part of the spectrum is the cause. ABS shells in several thicknesses were designed to provide shielding against the low energy proton component. These shells were then printed on-orbit and deployed over the port wall REM (SN2002, unit H10) in sequence in an effort to evaluate the dose impacts of the low-energy proton components as measured within the BEAM [4].

We performed a series of measurements with three different thicknesses of shielding material. In general, particles will impinge on the REM sensor somewhat equally over 4π. To ensure all particle trajectories see the same thickness of material the shield must constitute a spherical shell with the REM sensor at the center. In the ideal case the sensor would represent a single point inside of a spherical volume. The REM however is a planar sensor. To reduce path length effects the spherical shell was constructed to be much larger than the REM active size. The shield was also designed to be feasible to deploy and have the REM remain near its unshielded location. We estimated that a ratio of sphere diameter to REM linear size of at least a factor of 5 would be sufficient.

An estimate of the range (from the National Institute of Standards and Technology (NIST) PSTAR database) of protons in aluminum and polyethylene is shown in Figure 16. If one sets the material thickness to the predicted particle range at a given incident energy, then on average that particle will be shielded from the sensor. The vertical and horizontal black lines in Figure 16 mark the predicted range in polyethylene for 1, 3 and 10 mm. This corresponds to proton energies of roughly 9, 17 and 31 MeV. Thus for a 10 mm thick polyethylene spherical shell protons below 31 MeV will on average be shielded from the REM sensor. It's important to note here that what is also plotted in figure 16 is the stopping power in polyethylene and aluminum, which is used as a surrogate for LET. The measured LET for any energy particle is a distribution peaked at the most-probable value. The distribution average is approximately the average stopping power (see Figure 16). If we assume this is a valid surrogate for LET we expect that a 10 mm thick polyethylene shield will block protons with LET ¿= 1.7 keV/μm. This amounts to nearly 50% of the shaded blue region (starting from the top at 30 keV/μm) shown in the left plot in Figure 16. In order to cover the entire region in this study thicker shields would have to be constructed. Performing a differential measurement with two additional smaller thickness of 3 mm (2.9 keV/μm cuttoff) and 1 mm (5 keV/μm cutoff) would however facilitate extrapolation over a greater thickness range. Measurements at each of the proposed shield thicknesses for several weeks to 1-month duration can then be used to reconstruct spectra in the same fashion as those shown Figure 17.

The AMF lab on ISS was used to print three hemispherical shells of thickness 1.1 mm, 3.3 mm and 10 mm, the maximum thickness available by the AMF. The inner diameter of the shell was kept at 8 cm for all three different shell thicknesses. Measurements were taken from March, 2016 until December, 2017, with the 3.3 mm and 10 mm shells each deployed for about 200 days. The 1.1. mm shell was deployed for roughly 90 days (see Table 1 for details).

To better compare the spectra inside of BEAM, data were categorized into four

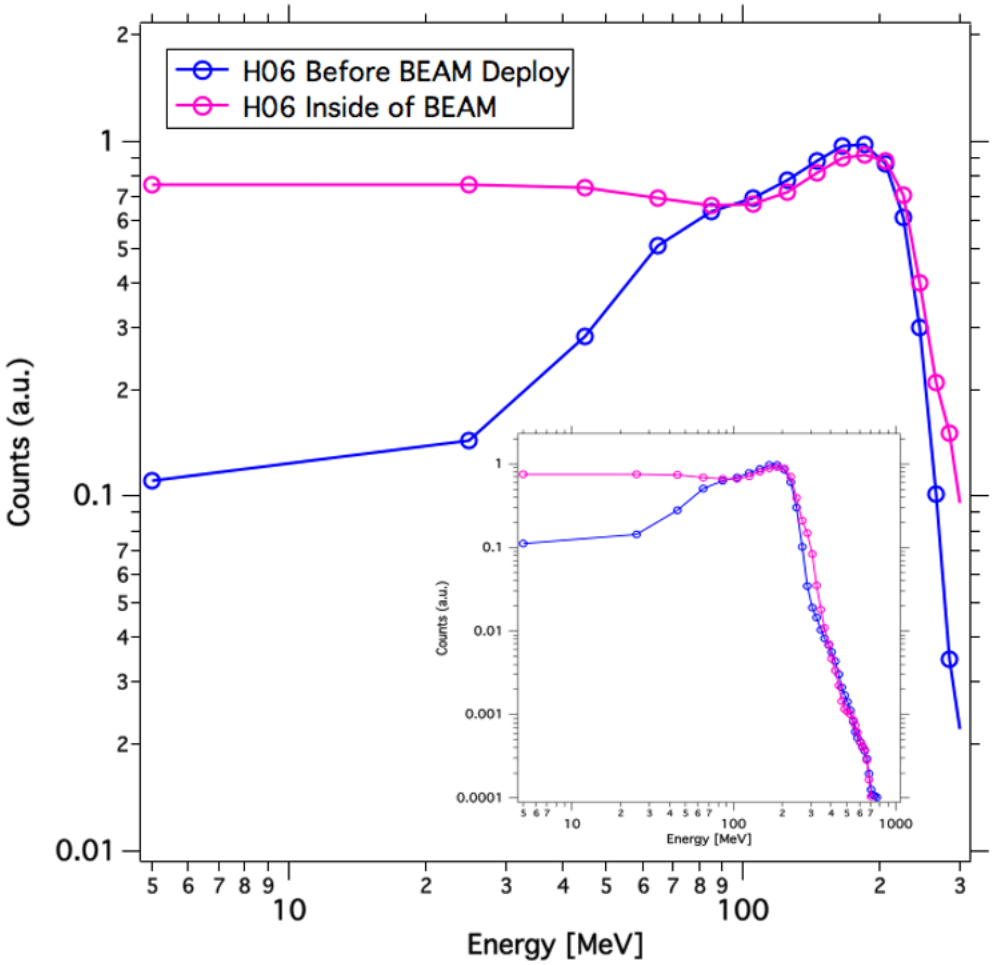

Figure 17. Constructed REM energy spectra inside of ISS and BEAM. (Blue) H06 data before deploy inside of BEAM. (Pink) H06 data after deploy inside of BEAM. Note the relatively large increase in counts for energies below 80 MeV. The inset shows the entire constructed spectra out to 900 MeV.

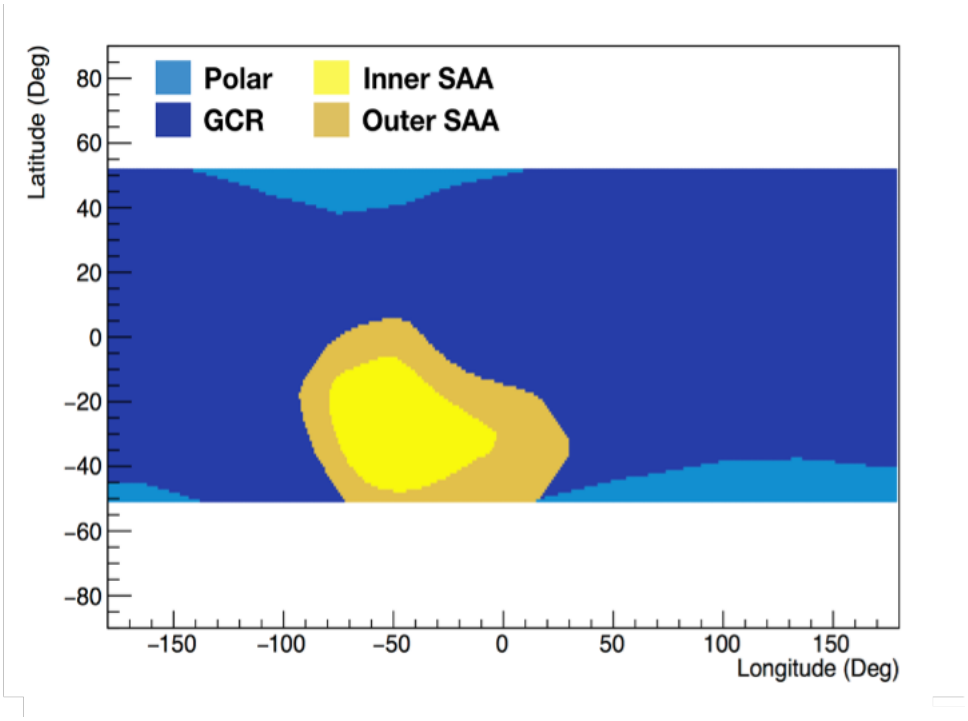

Figure 18. Location of regions used for BEAM spectral analysis.

regions based on latitude and longitude. These regions, shown in Figure 18, highlight environments that are dominated by:

- Low and higher energy trapped protons – respectively, the inner and outer SAA;
- Galactic Cosmic Rays (GCR) most and least modulated by the Earth's magnetic field – GCR and Polar.

The largest effect from the shells is seen for the "Outer SAA" region which is dominated by protons with energies lower than 20 MeV and can be effectively shielded by the thin shells. However, the effect from this on daily doses is negligible. This is because most of the SAA induced dose is from the "Inner SAA" region which has flux rates up to 40 times higher than those in the "Outer SAA". The Inner SAA is not significantly attenuated by the 3D printed shells as the protons spectrum inside BEAM is peaked around 40 MeV, which is sufficiently energetic to pass through the shells. It is also interesting to note that the unshielded fluxes are lower than some of the shielded fluxes. This can be due to changes in the SAA flux (population of the radiation belt, orientation and trajectory of ISS), as this trend can also be seen in the REM without shells.

Another way to look at potential changes is to look at the ratio between the BEAM H10 and H06 sensors since only the H10 sensor had the shielding shells installed. Results covering the timeline from pre-shell deploy through when the phase

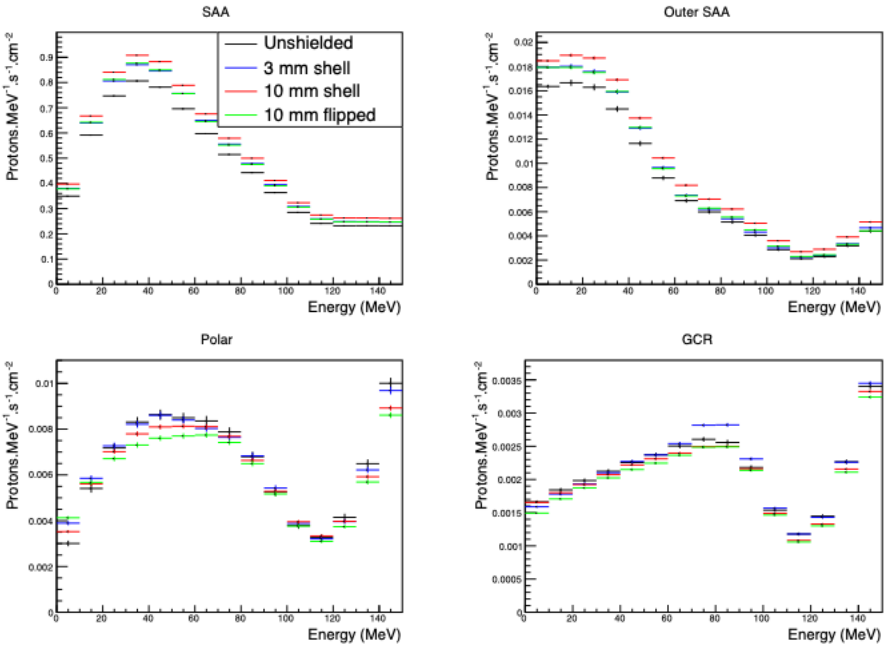

Figure 19. Spectra for REM without shell, by region and shell configuration.

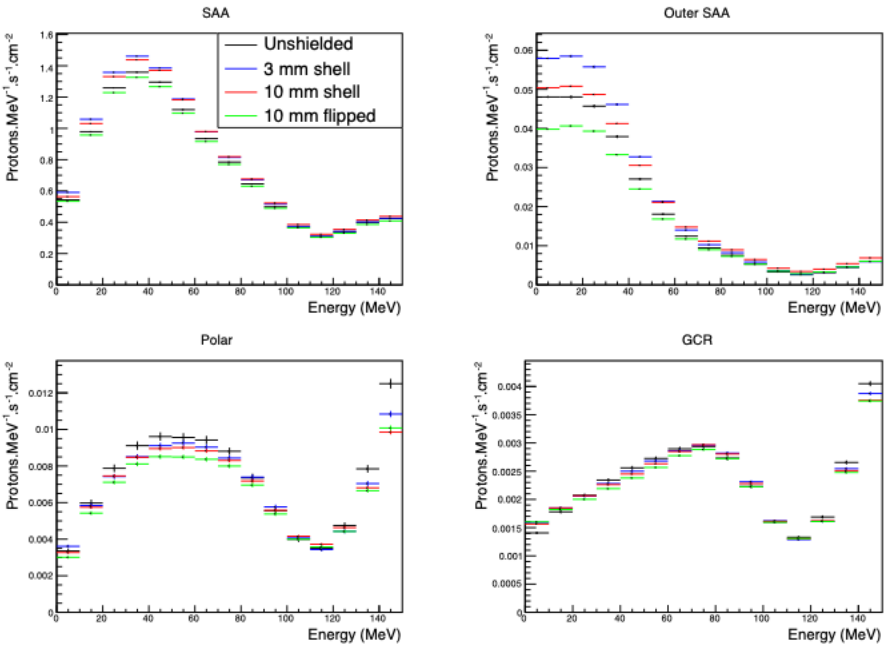

Figure 20. Spectra for REM without shell, by region and shell configuration.

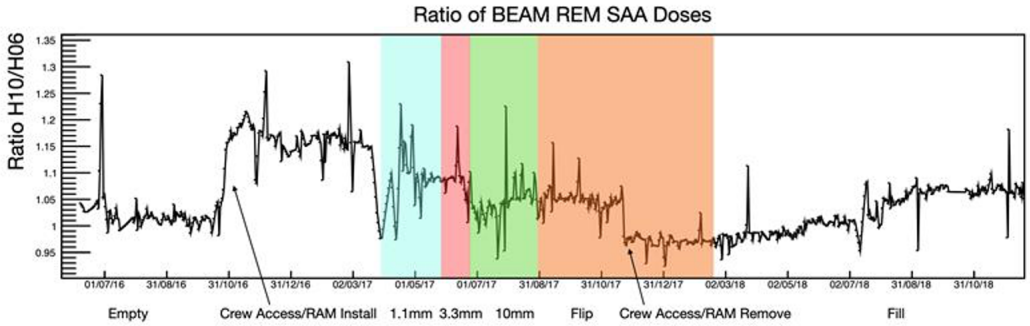

Figure 21. Ratio of SAA dose rate for H10 to H06 as a function of time. The shaded regions mark the different times frames of measurements where shells of different thicknesses were installed. The shielding shells were placed over the H10 sensor. The 10 mm shell was removed right before stowage started being added to the module.

when stowage started being added to the module is shown in Figure 21. The succession of shaded regions from blue to orange mark the various shell install periods starting with the 1 mm shell and ending with the 10 mm shell. It is clear here that there is in general a downward trend in the ratio with increase in shielding around the H10 sensor. As shielding increases one expects the H10 dose rate to decrease which would drive the ratio to lower values. However, the are two contributing effects observed which result in difficulty in assessing the effectiveness of the hemispherical shells. First, through January and February of 2016 (left side of figure), before the shells were installed, the ratio was trending at nearly a value of unity, implying that both sensor were roughly reading the same dose rate.

The largest effect from the shells is seen for the "Outer SAA" region which is dominated by protons with energies lower than 20 MeV and can be effectively shielded by the thin shells. However, the effect from this on daily doses is negligible. This is because most of the SAA induced dose is from the "Inner SAA" region which has flux rates up to 40 times higher than those in the "Outer SAA". The Inner SAA is not significantly attenuated by the 3D printed shells as the protons spectrum inside BEAM is peaked around 40 MeV, which is sufficiently energetic to pass through the shells. It is also interesting to note that the unshielded fluxes are lower than some of the shielded fluxes. This is likely due to changes in the SAA itself (population of the radiation belt, orientation and trajectory of ISS as it transits), as this trend can also be seen in the REM without shells.

4.3 Dose Trends During September 2017 SPE

The Solar Particle Event (SPE) in September 2017 was intense enough to be measured by a wide variety of instruments inside and outside the International Space Station (ISS) and on Earth's surface - classified as Ground Level Event (GLE) 72. In this section, we present measurements taken inside the habitable volume of ISS and inside of BEAM. The observed SPE-only contribution to the daily dose from

11 September to 12 September is summarized as:

- 2.5 mGy for REMH06 (11 - 12 September)
- 1.5 mGy for REMH10 (11 - 12 September)
- It is estimated that the additional absorbed dose per detector missed during the onset of the SPE at ISS (2 polar orbits) is on the order of 0.3 mGy in Si.

In this study, we use a model-based definition to distinguish between GCR and the transition/SAA region. In general, this allows for more direct comparisons of each environment by reducing the impact of localized shielding in the vehicle, detector capabilities, and detector-based definitions of the environment, e.g. event rate based.

As implemented, we use the internal geomagnetic field as generated by IGRF12 (International Geomagnetic Reference Field). For greater accuracy, we directly use ISS trajectory as inputs to the calculation of geomagnetic field intensity - B - and Mc Ilwain L-shell values. ISS trajectory is calculated using TLEs (Two Line Elements) and SGP4 (Simplified General Perturbation model). The transition/SAA region is simply defined by $|B| < 23$ μT and $L < 3$ [3], and is shown in figure 22.

All of the REMs in BEAM and in the habitable volume of ISS were active during the SPE as observed at ISS, i.e. 11 September. Unfortunately, the two REMs in BEAM were not operational during the onset of the event. Note that the reduced uptime observed in Figure 23 is typical given the current infrastructure; an analysis of the data including backfilled measurements (to recover uptime) is further described in Subsection 4.3.3.

4.3.1 Overview of SPE Events

September 2017 was a busy time on the sun, with a class X9.3 solar flare occurring at 12:24 UTC on 06 September, accompanied by a Coronal Mass Ejection (CME) and Solar Particle Event. A X8.2 flare took place later, at 16:06 UTC on 10 September with another fast CME, resulting in an Energetic SPE with a higher-energy proton component relative to the 06 September SPE. This second SPE was large enough to disturb the geomagnetic fields in LEO, reducing cutoff rigidities and pushing lower-energy protons into lower L-shells. This typically results in increased proton fluxes in GCR, which are clearly visible inside the Columbus Laboratory, where ISS-RAD (Radiation Assessment Detector) was also located. ISS-RAD saw a clear softening of the proton spectrum in GCR with a significant intensification of the flux (shown in the next figure). At its maximum peak, the lowest stopping proton bin - [20, 35) MeV - was 5 times more intense than the nominal GCR environment.

A time series of GOES proton flux [5], stopping proton flux in ISS-RAD (located in Columbus), and GCR measurements from all of the active REMs are shown in Figure 25. In addition, mass shielding distributions based on available vehicle models are shown for Columbus (J02) and BEAM (H10 and H06) REM instrument locations. From Figure 24, it can be seen that the mass shielding in BEAM is much lower than in the Columbus module.

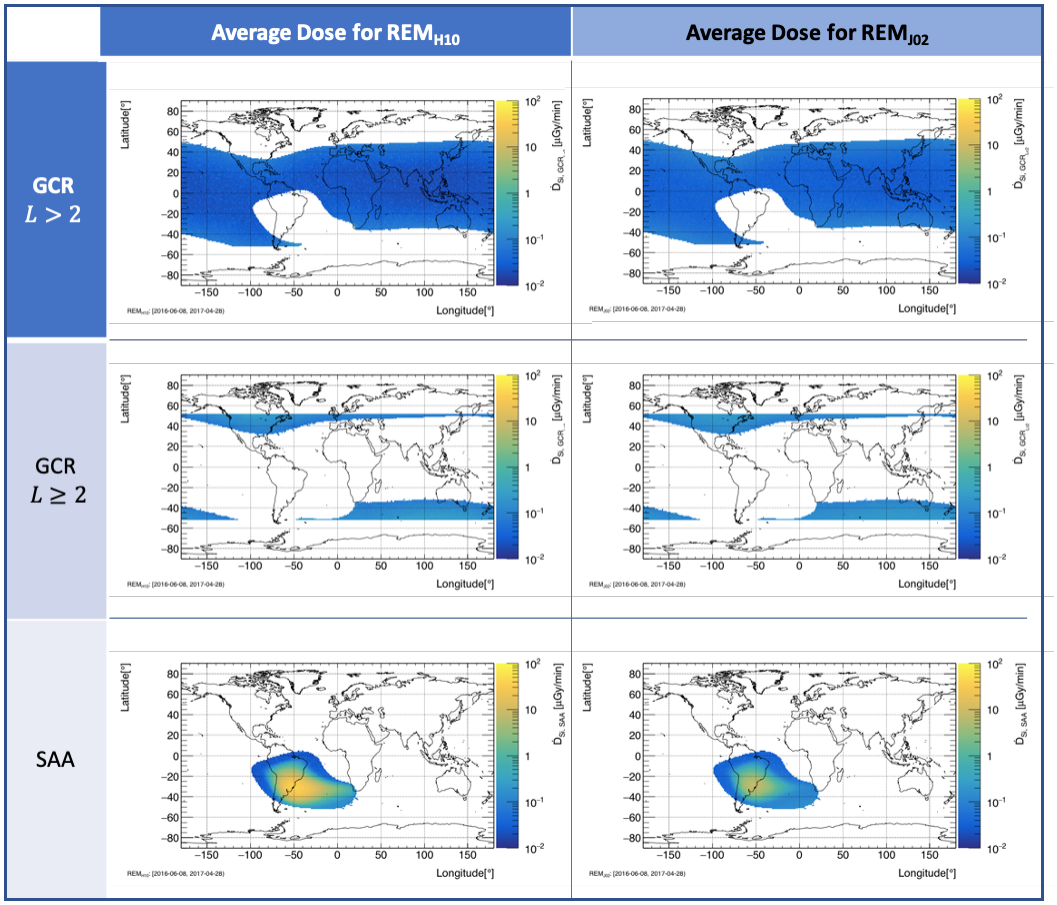

Figure 22. Visual definitions of the LEO environment for GCR with further separation by L-shell values - $L < 2$ and $L \geq 2$ - and the SAA are shown for REMH10 and REMJ02.

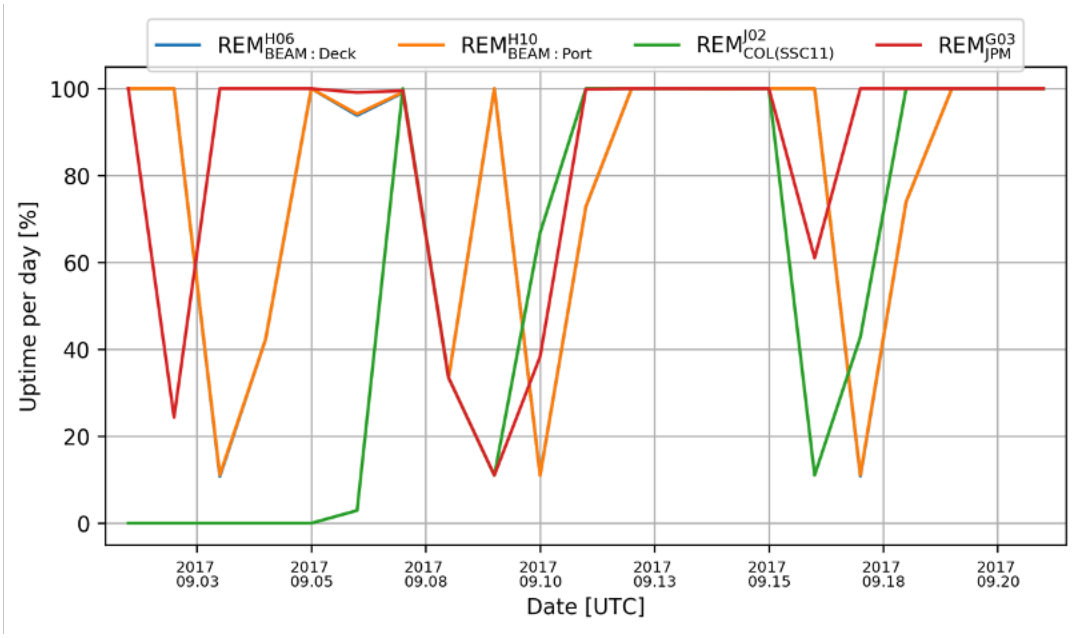

Figure 23. REM uptime per day between 2017-09-01 and 2017-09-22.

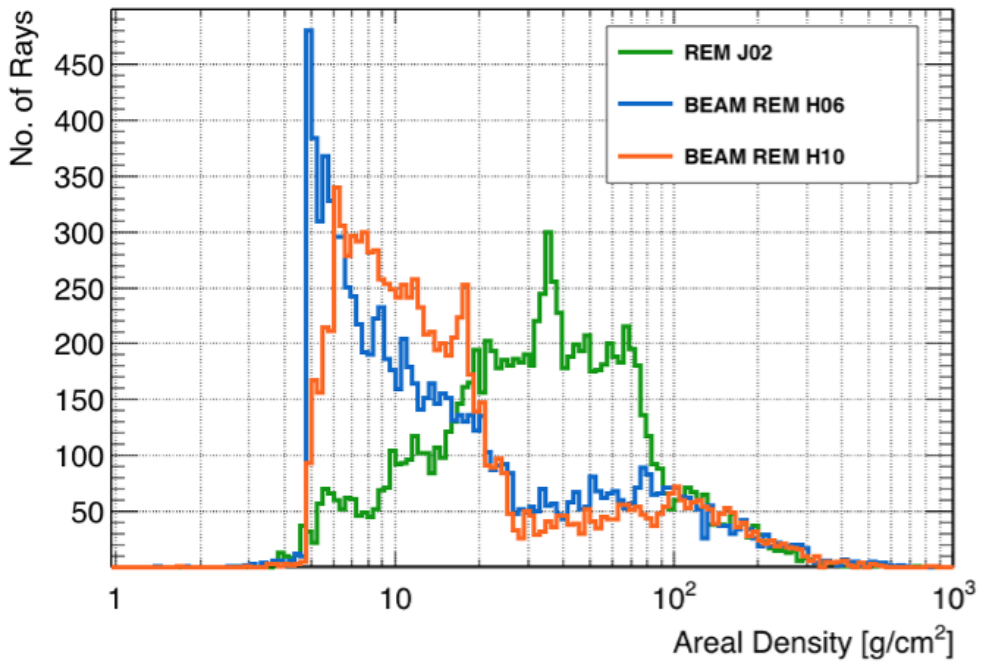

Figure 24. Comparison of shielding distributions inside of Columbus (REM J02) and BEAM (REM H06/H10).

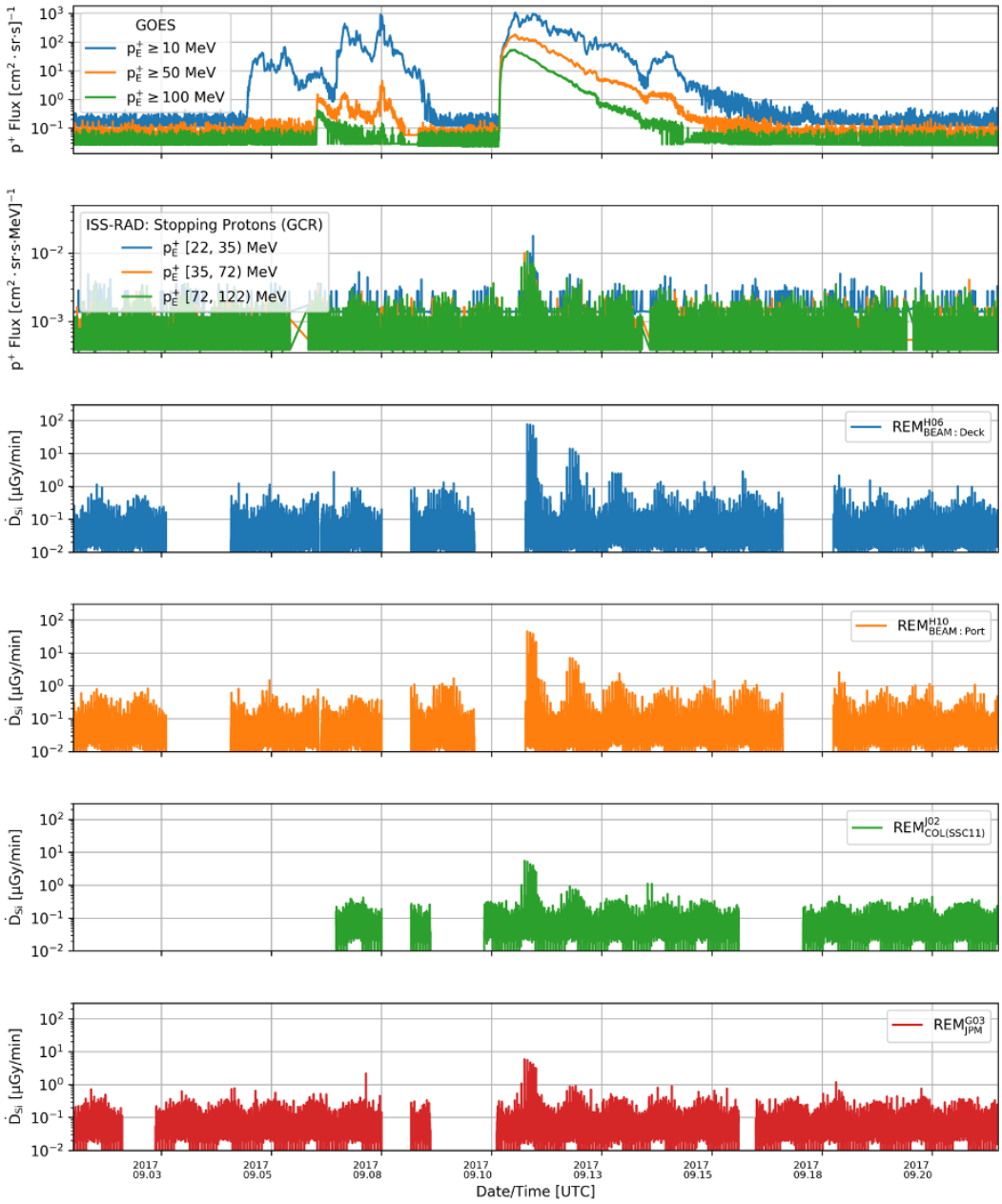

Figure 25. GOES flux (top), followed by stopping proton flux in the ISS Columbus module as measured with RAD for GCR (described in the GCR/SAA Identification sub-section), followed by absorbed dose rates in Si for the non-SAA environment, as measured by the two REMs in BEAM (H06, H10) and REMs in the Columbus Laboratory (J02) and JPM (G03).

4.3.2 Energy Loss Spectra

Energy loss spectra before and during the SPE are shown in Figure 26. One can clearly see the hardening of the dE/dx spectra (indicating softening of kinetic energy spectra). One can also see that the SPE primarily impacted the GCR region in higher L shells. The most significant change in GCR with $L \geq 2$ is observed in REMH06, where flux in energy loss around 8 keV/μm (in Si) is 80X higher relative to the nominal environment.

All instruments are susceptible to downtime which can be caused by a number of reasons, including, power outages, relocates, et cetera. REMs are parasitic to SSCs which frequently go through nominal reboots and user logout/logins which typically means that there is significantly reduced data coverage on weekends.

A backfilling algorithm has been developed that allows us to estimate the dose rate (and other observables of interest) as function of time and ISS trajectory [2,3]. In short, the algorithm generates a set of multi-dimensional histograms for the observable of interest in bins of latitude, longitude, altitude, and time. ISS position can be calculated (or looked up) for any timestamp and then used to look up the average observable - dose rate in this study. Another extension of this algorithm is that we can artificially mask real data to estimate the nominal radiation environment inside ISS. Backfilled data, while a powerful tool for post mission assessments, is not a surrogate for real data; it is only as functional as the input data and can still be subject to rapidly changing environments.

4.3.3 SPE Dosimetry Summary

Backfilled data have been generated for these REMs with and without a mask applied to the SPE period: 11-13 September. The SPE-only contribution can be estimated by subtracting the backfilled estimate (with the mask applied) from the measured data. Shown in Table 6. In general, the results show that:

- Average SPE Dose (D_{Si}) in BEAM is 2 mGy.
  - 2-3 times more dose incurred relative to a nominal day in BEAM.
  - Note that the early onset of the SPE was not measured by these REMs; 2 polar passes occurred prior to the detectors going online. The average dose per measured pass in REMH10 is roughly 0.15 mGy. As a conservative estimate, we can include this dose rate to the SPE-only contribution.
- Average Habitable volume of ISS Dose (D_{Si}) is 0.25 mGy.
  - Roughly 0.5 times more dose incurred relative to a nominal day on ISS; comparable to other operational instruments, e.g. ISS-RAD.

The effect of backfilling on data can be seen in Figure 11. For comparison, see Figure 10 showing the data without backfilling applied. GOES proton flux and cumulative absorbed dose per day (in Si) with backfilling for the days surrounding the SPE are shown in Figure 29.

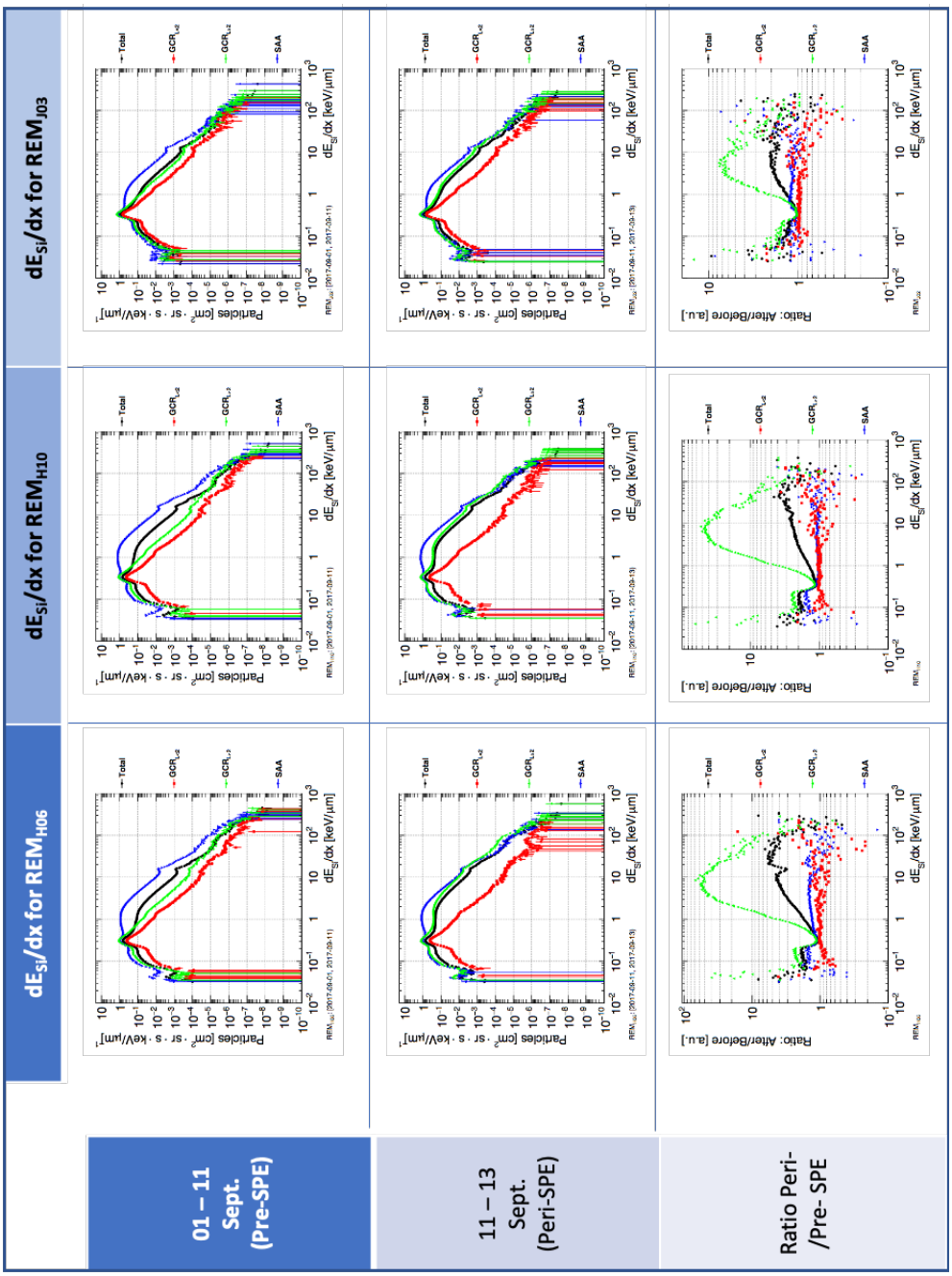

Figure 26. Energy loss spectra (in Si) for the REMs in BEAM (H06 and H10) and JPM (G03) pre- and peri-SPE. A ratio of the spectra (peri/pre) is provided in the last row to show the relative change to the environment. Energy loss spectra are categorized by the SAA and GCR ($L < 2$ and $L \geq 2$) environments (as discussed in the GCR/SAA Identification sub-section). Note that these spectra are normalized to the total amount of time in each environment and therefore will not add up to the total.

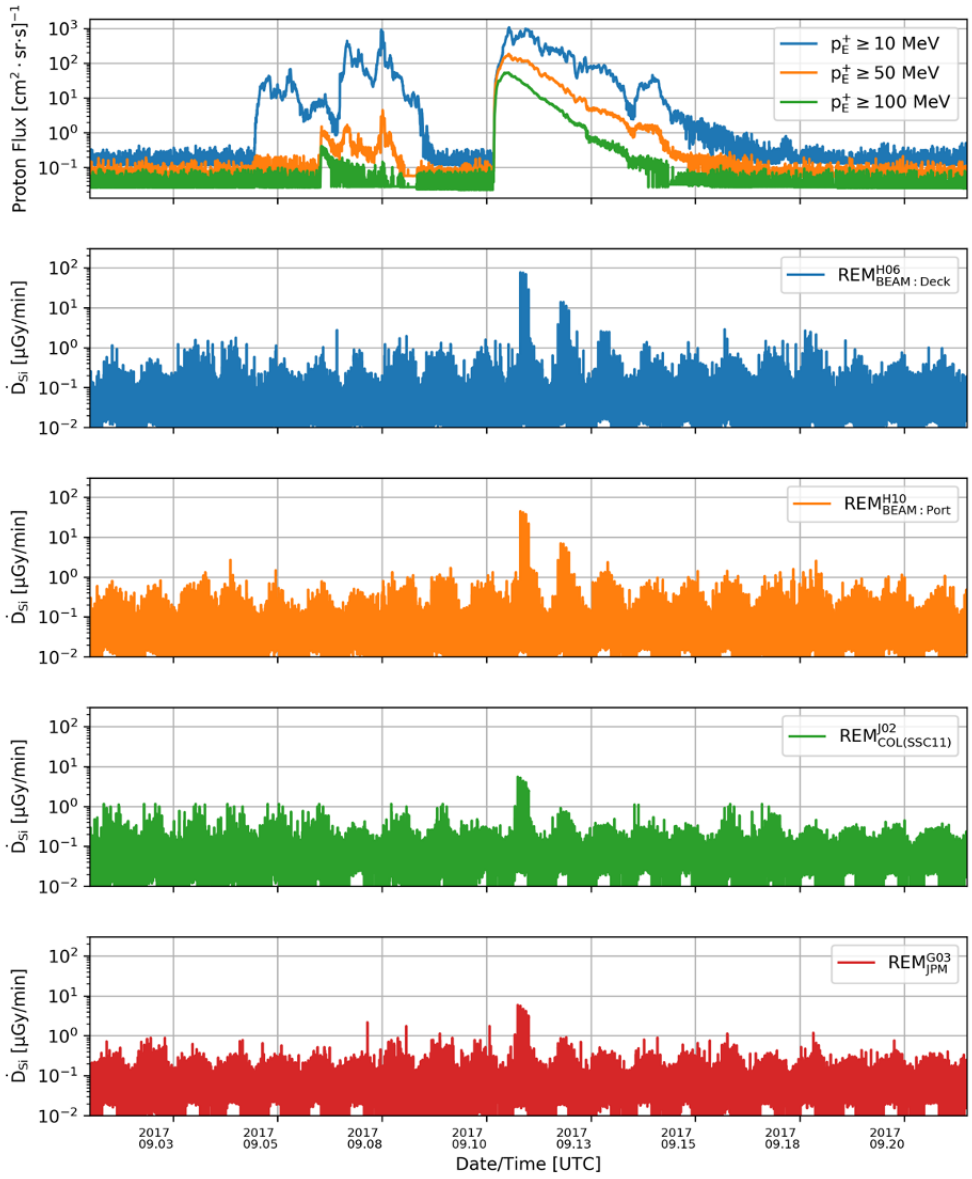

Figure 27. GOES flux in the upper most panel, followed by the measured and backfilled absorbed dose rates in Si for the non-SAA environment with the two REMs in BEAM (H06, H10) and REMs in the Columbus Laboratory (J02) and JPM (G03).

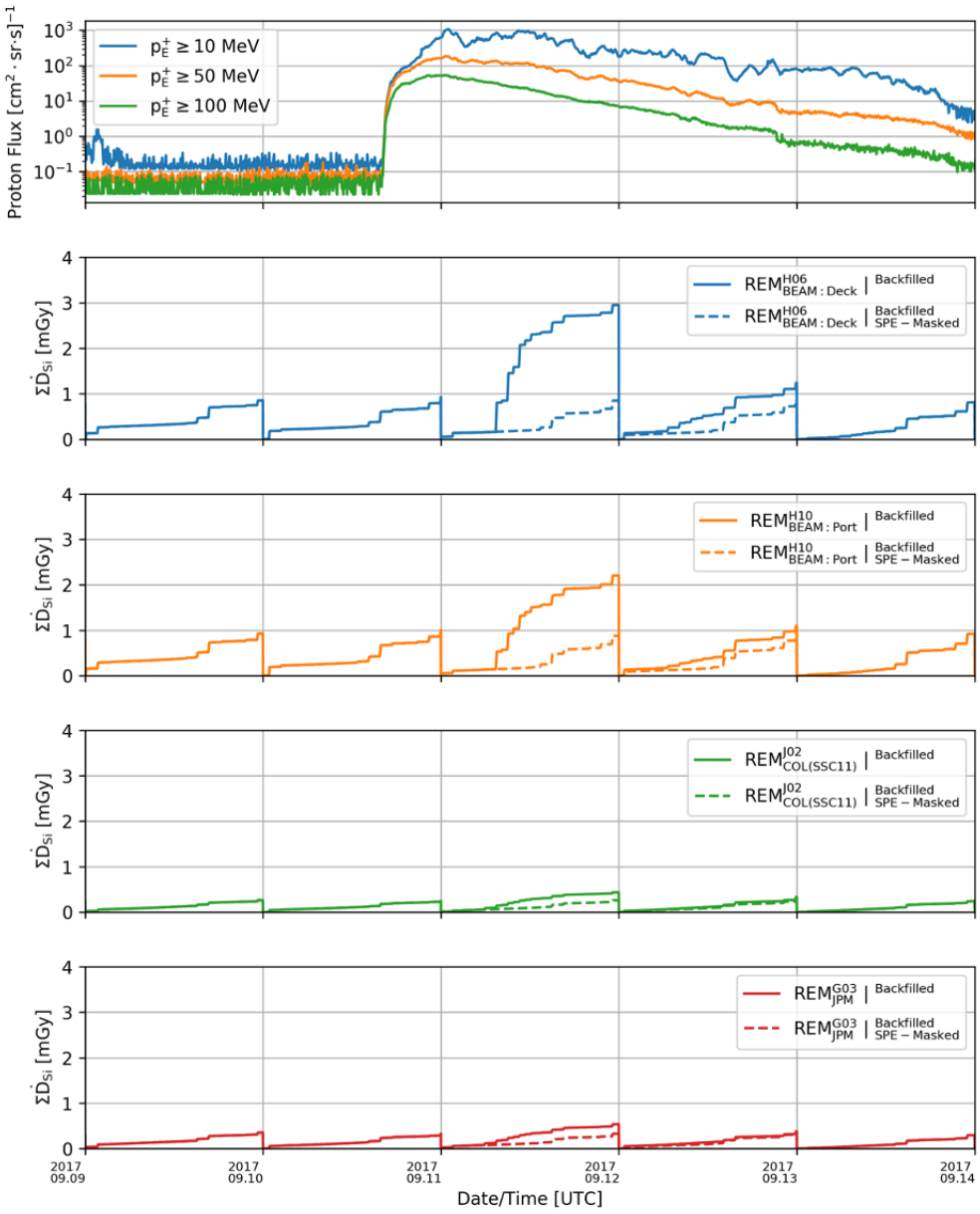

Figure 28. GOES proton flux in the uppermost panel, followed by the cumulative absorbed dose in Si per day for the total combined environment using measured and backfilled data from the two REMs in BEAM (H06, H10) and REMs in the Columbus Laboratory (J02) and JPM (G03). Dashed lines indicate measured and backfilled data after masking out 11-13 September to estimate the nominal radiation environment.

Table 7. Cumulative absorbed daily dose in Si for the REMs in BEAM and the habitable volumes of ISS. Note that the bolded values indicate data that are measured/backfilled; non-bolded measured/backfilled after masking 11-12 September; bolded values highlight the difference, i.e. SPE's contribution. *Add 0.3 mGy for missing data.

Daily Absorbed Dose in Si [mGy]						
	9 Sept.	**10 Sept.**	**11 Sept.**	**12 Sept.**	**13 Sept.**	**12 Sept.**
H06+PE						
Total	0.85	0.93	2.95	1.24	0.81	0.89
SPE Masked	0.85	0.93	0.85	0.86	0.81	0.89
SPE Only*			**2.10**	**0.38**		
H10						
Total	0.93	1.0	2.20	1.10	0.92	0.92
SPE Masked	0.93	1.0	0.88	0.92	0.92	0.92
SPE Only*			**1.32**	**0.18**		
J02 (COL)						
Total	0.26	0.24	0.44	0.34	0.24	0.26
SPE Masked	0.26	0.24	0.26	0.27	0.24	0.26
SPE Only			**0.18**	**0.07**		
G03 (JPM)						
Total	0.35	0.32	0.54	0.38	0.30	0.32
SPE Masked	0.35	0.32	0.33	0.35	0.30	0.32
SPE Only		**0.21**	**0.03**			

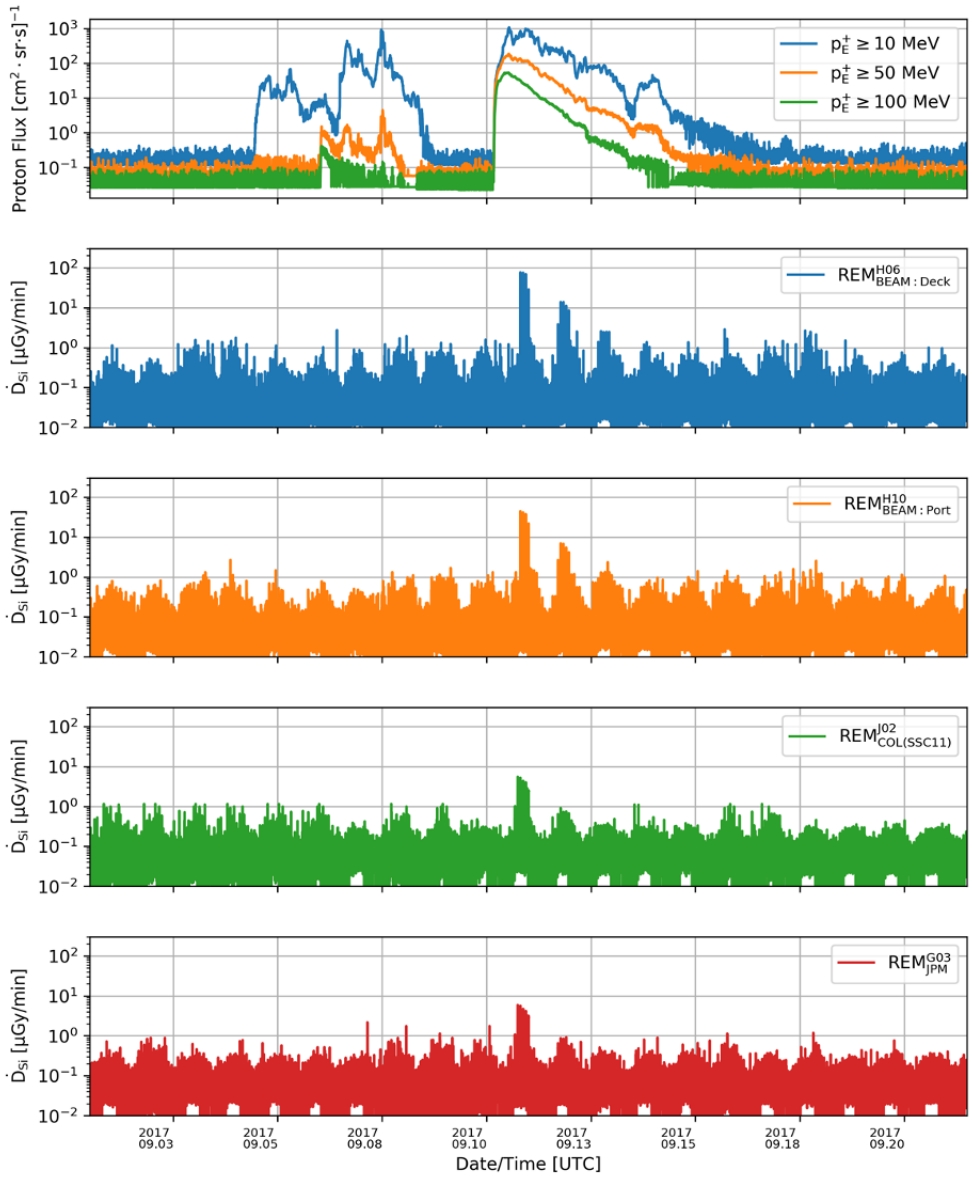

Figure 29. GOES flux in the upper most panel, followed by the measured and backfilled absorbed dose rates in Si for the non-SAA environment with the two REMs in BEAM (H06, H10) and REMs in the Columbus Laboratory (J02) and JPM (G03).

5 Placement Correction - Deck to Overhead

Deployment of the H06 unit was planned for the BEAM deck centerline location, with shielding analysis and dosimetry predictions generated for the port and deck locations. Subsequent imagery from on-orbit BEAM operations showed that the H06 unit was deployed to the BEAM overhead centerline. Comparison of the BEAM deck and BEAM overhead centerline location raytrace results are shown in figure 30. The shielding distributions show little devation, which is unsurprising given the symmetry of the BEAM design along the central axis, and the dosimetry projections remain valid for the as-deployed overhead location.

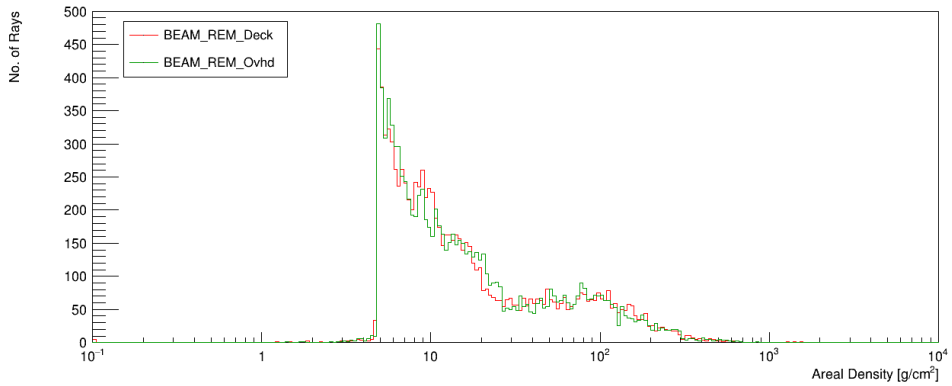

Figure 30. Comparison between the overhead and deck deploy locations as an equivalent aluminum thickness in g/cm^2.

6 REM Dose Rate Trends - BEAM w/Stowage

Radiation Environment Monitor payload hardware was deployed in the BEAM module on 07 June, 2016. REM serial number 2002 (ChipID H10-W0099) was deployed on the port wall midline of the module. This unit was relocated from Node1. Data from this unit stopped acquisition in Node1 at GMT 2016/159 08:17, and data acquisition resumed in the BEAM at GMT 2016/159 09:59. REM serial number 2003 (ChipID H06-W0099) was deployed on the overhead wall midline. The unit was relocated from Node2, with data acquisition halting in Node2 at GMT 2016/159 08:13 and resuming at GMT 2016/159 09:10 in BEAM.

Initially, the units were expected to have been deployed on the port and deck wall midlines, however subsequent ISS imagery and analysis revealed that unit 2003 (H06) was actually deployed at the overhead midline location. Both units were connected to SSC24 via the BEAM instrumentation cable which utilized a hatch feedthrough to allow operation while the BEAM hatch was closed. The BEAM instrumentation cable also supported the impact sensor system as well as other BEAM sensor system data acquisition on SSC24.

Table 8. BEAM Stowage Build-up as reported by ISS ISO

Date	GMT	Mass [kg]	Mass [lbs]
02/20/18	2018/051	464.16	1023.30
05/23/18	2018/143	488.89	1077.82
09/18/18	2018/261	614.44	1354.60
01/29/19	2019/019	1439.32	3173.16

Data from unit 2003 halted on 31 December 2018, and the unit has remained non-responsive since that time. The unit is assumed to have become disconnected inside the BEAM as a result of stowage operations within the module, though hardware failure cannot be ruled out.

Data is shown through Aug 10, 2019. A single pixle in H10-W0099 began producing very high single hit values which is indicative of a threshold shift locally in the pixel. This 'hot pixel' requires and update to the calibration files to apply a mask for this single pixel input. In late July 2019, this pixel in unit 2002 (pixel matrix location [59,240]) began showing consistent, single-hit activity with reported energies of around 100 keV, and by mid to late August this had gradually increased to consistent single-pixel readings of over 2MeV. While such data points are not unheard of, a consisently active pixel of this magnitude shows the response of this pixel is unreliable. Left unmasked, this pixel input shifts measured dose rates considerably higher, and correction requires reprocessing of the raw data to apply the pixel mask. The REM payload activities are concluded, and the resources necessary to reprocess data are no longer avaiable, so the data set for this report was truncated at Aug 10, 2019.

6.1 BEAM Stowage Operations

Stowage Bags were deployed in BEAM, allowing accumulation of stowage mass within the module. Stowage operations began in early 2018, with the build-up mass values reported through stowage operations meeting presentations (see table 8). Dates provided are estimated and mass changes are expected to immediately follow BEAM Ingress activities since the module hatch is nominally closed. Ingress activities are shown in table 4. Details regarding mass distribution over time within the module are unavailable.

6.2 Stowage Buildup and Data Source

Data for the stowage build-up was provided by Ryan East, an ISS Inventory and Stowage Officer (ISO), and from information contained in ISS Chit 15823 relating to BEAM stowage outfitting. Additional information on stowage containers can be obtained from the ISS Resupply Stowage Platform 1 Interface Control Document (JSC-28169). BEAM activity timeline information was collected from the ISS OPTIMIS scheduling tool.

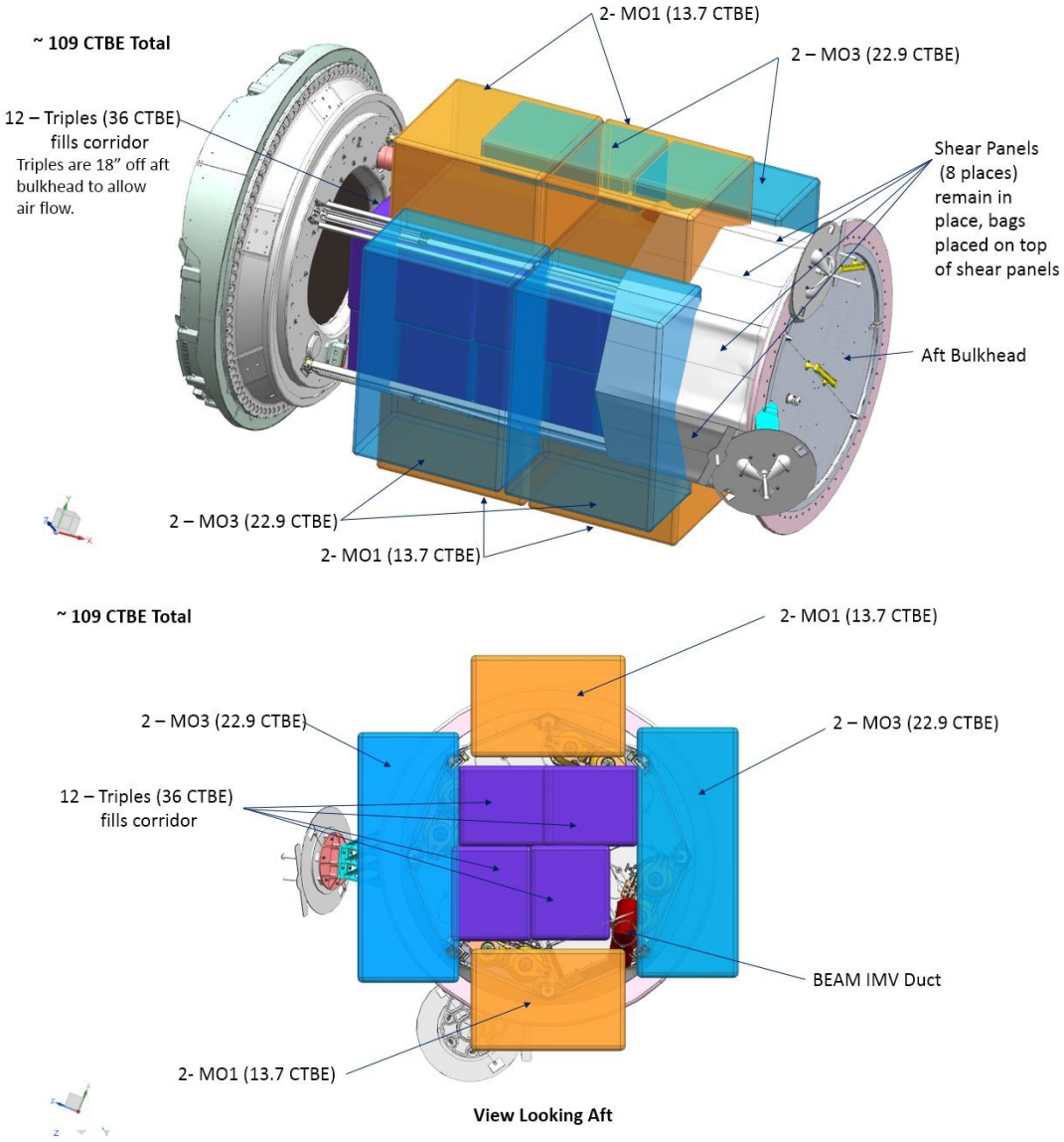

Figure 31. Stowage configuration layout as reported by Operations Support Officer.

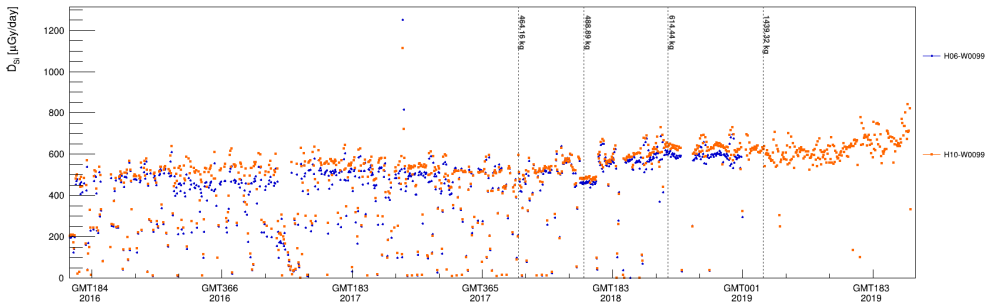

Figure 32. Daily dose rates in BEAM since 2016 with mass activities indicated. Enhanced dose rates resulting from the Sept 2017 SPE are also visible in the plot. Acquisition softwrae updates in 2018 and 2019 yeilded noticably higher instrument live-time and more consistent daily dose rates as percent daily coverage increased.

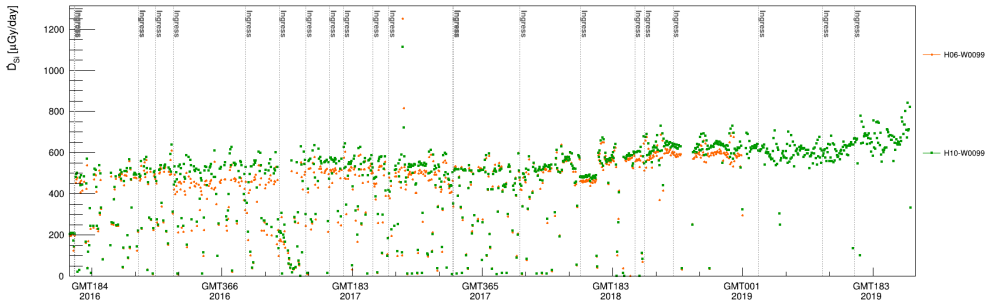

Figure 33. Daily dose rates in BEAM since 2016 with module ingress (hatch-open) activities indicated.

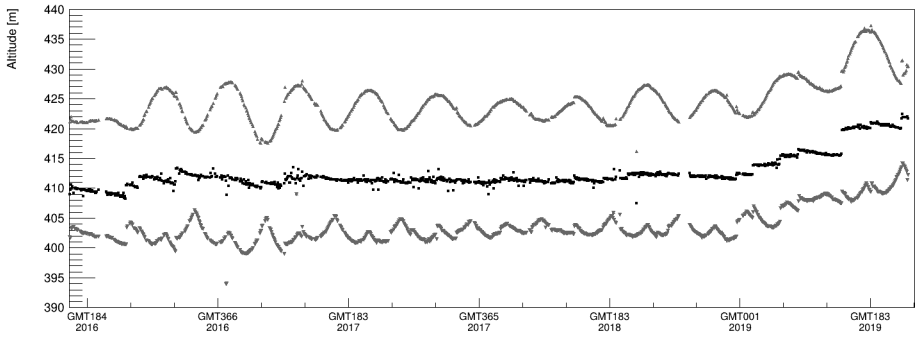

Figure 34. Daily average, maxiumum, and minimum altitudes for ISS as populated in the REM data format using SGP4 and ISS TLE data since June 2016

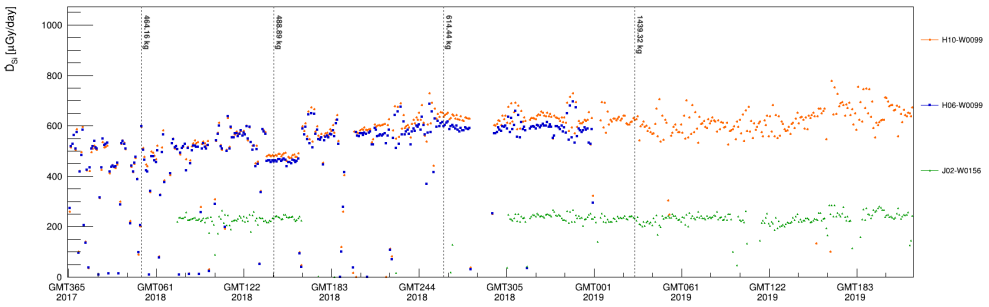

Figure 35. Dose rates per day for BEAM and Columbus REM units during 2018 and 2019.

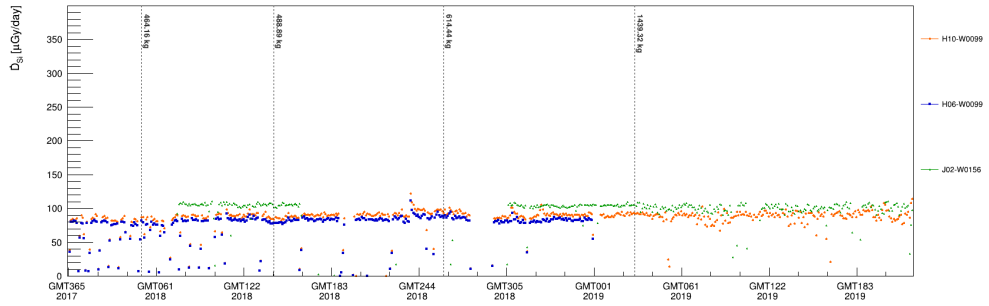

Figure 36. Daily dose rates attributed to locations outside the SAA for BEAM and Columbus REM units during 2018 and 2019.

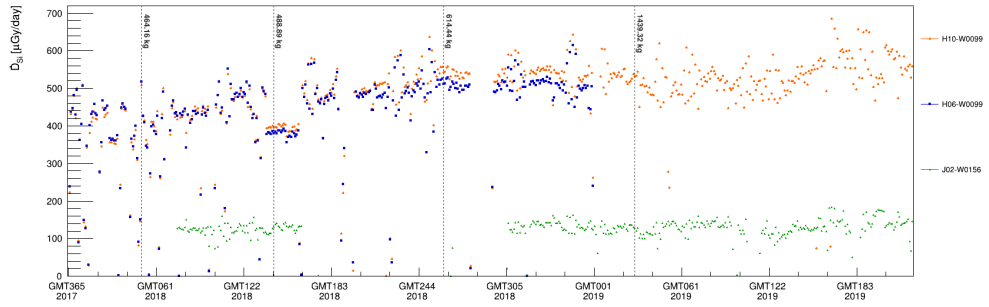

Figure 37. Daily dose rates attributed to orbital locations within the South Atlantic Anomaly for BEAM and Columbus REM units during 2018 and 2019.

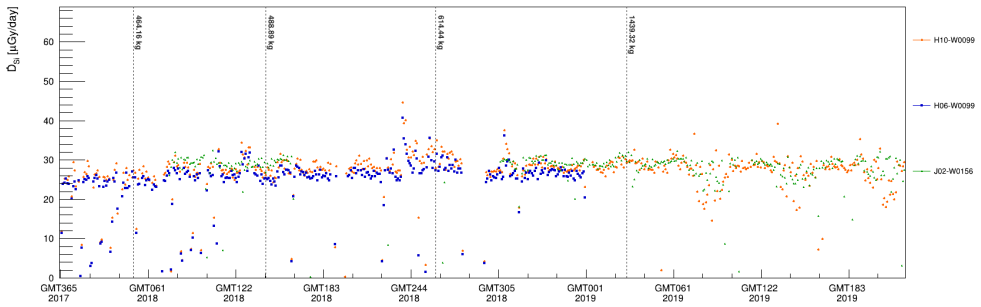

Figure 38. Daily dose rates attributed to orbital locations in the geomagnetic cusp regions for BEAM and Columbus REM units during 2018 and 2019.

6.3 Dose Rate Trends

Comparison of mass values and dose rates outside of the South Atlantic Anomaly show no dependence on mass changes within BEAM. Comparisons of SAA doses and total stowage mass indicate two possible time periods (May 2018 and Sept 2018) where module ingress and subsequent mass reports indicate possible impact on dose rates. However, there are no ingress activities and no clear indication of mass change in the timeline where the dose rate trend changes again following these two possible periods of mass impact, which indicates that other factors such as altitdue, vehicle orientation, or other operations activites unrelated to BEAM stowage were the cause of these changes in dose rate trends.

7 Conclusions

Measurements report during this observation period continue to show daily dose trending that is $\approx$ 3X higher than daily dose with REM sensors in the US LAB model. Analysis of LET spectra imply that the increased dose is likely coming from protons with energy up to roughly 150 MeV during passes through the SAA. First flux spectra generated from REM measurements are in agreement with LET spectra.

RAM measurements collocated with REM sensors in BEAM show on average nearly the same daily dose with a maximum difference of 16%. It is not unreasonable to expect at least a 10% uncertainty in any given measurement and thus the RAM and REM measurements are in relatively good agreement. Across all 6 BEAM RAM measurements we observed a consistent trend of higher average daily dose than seen with RAMs in other ISS modules, again in agreement with what has been observed to date with REM measurements.

References

1. Rios, R., (2017), Comparison of Silicon-Based Detectors, 22nd Monitoring on the International Space Station, 05-07 September 2017, Turino, Italy

http://www.wrmiss.org/workshops/twentysecond/Rios.pdf

2. Rios, R., (2017), Backfilling Methodology, SRAG-COM-PHYS-2017-003.

3. Rios, R. (2018), Timepix in ISS Operations, Use of Timepix in Space Meeting at CERN, 09 March, 2018, Geneva, Switzerland. https://indico.cern.ch/event/694586/contributions/2928562/attachments /1615849/2567997/timepix_in_iss_ops.pdf

4. Napoli, M., (2017), REM Enclosures On-Orbit Printing Report, Made In Space, Inc. Technical Report No. AMF03094 (AMF03086A), Revision A, August 2017

5. Geostationary Operational Environmental Satellite (GOES), https://www.ngdc.noaa.gov/stp/satellite/goes/.

6. Stoffle, N., et al (2015), Timepix-based Radiation Environment Monitor Measurements Aboard the International Space Station, Nuclear Instruments and Methods in Physics Research Section A, Vol 782.

Appendix A

Nomenclature

Table A1. Standard conventions, acronyms and units.

AES	Advanced Exploration Systems (Program under NASA HEOMD)
COTS	Commercial Off-The-Shelf
$\dot{D}(t)$	Dose rate as a function of time
EVA	Extra-Vehicular Activity
HEOMD	Human Exploration and Operations Mission Directorate
IGRF	International Geomagnetic Reference Field
L	McIllwain L-shell Value
SPE	Solar Proton Event
SSP	Space Station Program

REPORT DOCUMENTATION PAGE	Form Approved OMB No. 0704–0188

1. REPORT DATE *(DD-MM-YYYY)*	2. REPORT TYPE	3. DATES COVERED *(From - To)*
01-09-	Technical Publication	

4. TITLE AND SUBTITLE	5a. CONTRACT NUMBER
Final Report on Radiation Measurements Performed Inside of the BEAM Module	5b. GRANT NUMBER
	5c. PROGRAM ELEMENT NUMBER

6. AUTHOR(S)	5d. PROJECT NUMBER
C. A. Kelleher	5e. TASK NUMBER
	5f. WORK UNIT NUMBER

7. PERFORMING ORGANIZATION NAME(S) AND ADDRESS(ES)	8. PERFORMING ORGANIZATION REPORT NUMBER
NASA Johnson Space Center	L–

9. SPONSORING/MONITORING AGENCY NAME(S) AND ADDRESS(ES)	10. SPONSOR/MONITOR'S ACRONYM(S)
National Aeronautics and Space Administration Washington, DC 20546-0001	NASA
	11. SPONSOR/MONITOR'S REPORT NUMBER(S) NASA/TP—-20240011436

12. DISTRIBUTION/AVAILABILITY STATEMENT

Unclassified-Unlimited
Subject Category
Availability: NASA STI Program (757) 864-9658

13. SUPPLEMENTARY NOTES

An electronic version can be found at http://ntrs.nasa.gov.

14. ABSTRACT

15. SUBJECT TERMS

dose,radiation dose,beam,international space station,ISS,dosimetry,timepix,minipix

16. SECURITY CLASSIFICATION OF:			17. LIMITATION OF ABSTRACT	18. NUMBER OF PAGES	19a. NAME OF RESPONSIBLE PERSON
a. REPORT	b. ABSTRACT	c. THIS PAGE			STI Information Desk (email: help@sti.nasa.gov)
U	U	U	UU		19b. TELEPHONE NUMBER *(Include area code)* (757) 864-9658